Lipophilic Guanylhydrazone Analogues As Promising Trypanocidal Agents: An Extended SAR Study

Vasiliki Pardali[a], Erofili Giannakopoulou[a], Dimitrios-Ilias Balourdas[a], Vassilios Myrianthopoulos[a], Martin C. Taylor[b], Marina Šekutor[c], Kata Mlinarić-Majerski[c], John M. Kelly[b], and Grigoris Zoidis[a,*]

[a]School of Health Sciences, Faculty of Pharmacy, Department of Pharmaceutical Chemistry, National and Kapodistrian University of Athens, Panepistimiopolis-Zografou, GR-15771 Athens, Greece; [b]Department of Infection Biology, London School of Hygiene and Tropical Medicine, Keppel Street, London WC1E 7HT, UK; [c]Department of Organic Chemistry and Biochemistry, Ruđer Bošković Institute, Bijenička cesta 54, 10 000 Zagreb, Croatia

*Corresponding author:

Prof. Grigoris Zoidis (zoidis@pharm.uoa.gr)

Keywords: Adamantane, *S*-adenosylmethionine decarboxylase (AdoMetDC), guanylhydrazones, structure-activity relationships, trypanocidal agents, Kernel-based Partial Least Squares regression, SZmap, Hydration analysis, Docking-scoring calculations

Abstract

In this report, we extend the SAR analysis of a number of lipophilic guanylhydrazone analogues with respect to *in vitro* growth inhibition of *Trypanosoma brucei* and *Trypanosoma cruzi*. Sleeping sickness and Chagas disease, caused by the tropical parasites *T. brucei* and *T. cruzi*, constitute a significant socioeconomic burden in low-income countries of sub-Saharan Africa and Latin America, respectively. Drug development is under-funded. Moreover, current treatments are outdated and difficult to administer, while drug resistance is an emerging concern. The synthesis of adamantane-based compounds that have potential as antitrypanosomal agents, is extensively reviewed. The critical role of the adamantane ring was further investigated by synthesizing and testing a number of novel lipophilic guanylhydrazones. The introduction of hydrophobic bulky substituents onto the adamantane ring generated the most active analogues, illustrating the synergistic effect of the lipophilic character of the C1 side chain and guanylhydrazone moiety on trypanocidal activity. The *n*-decyl C1-substituted compound **G8** (R = $C_{10}H_{21}$) proved to be the most potent adamantane derivative against *T. brucei* with activity in the nanomolar range (EC$_{50}$=90 nM). Molecular

simulations were also performed to better understand the structure-activity relationships between the studied guanylhydrazone analogues and their potential enzyme target.

1. Introduction

Neglected tropical diseases (NTDs) constitute a diverse group of chronic bacterial, protozoan, fungal, viral and helminth infections [1,2] in 149 countries worldwide [3]. It is estimated that more than a billion people — one-sixth of the world's population, are affected by NTDs in tropical and sub-tropical regions. These infections are considered to be one of the leading causes of high morbidity and mortality in underdeveloped countries [4]. Leishmaniasis, Human African Trypanosomiasis (HAT), Chagas disease and malaria are the most serious and prominent protozoan infections, accounting for the highest death toll among the existing NTDs annually [5,6]. In this review, we will focus on the two trypanosomiases, HAT and Chagas disease, caused by protozoan parasites of the genus *Trypanosoma*.

1.1 Human African trypanosomiasis

Human African trypanosomiasis (HAT), also known as sleeping sickness, is a vector-borne disease that affects poor populations in the African continent. It is caused by infection with the protozoan parasite *Trypanosoma brucei* and is transmitted by the bite of tsetse flies of the genus *Glossina* [7]. The disease is found in 36 countries of sub-Saharan Africa and about 65 million people are at risk of developing the infection [8].

Two morphologically identical subspecies of *T. brucei* are responsible for the onset of the disease in humans. They display a different host range, exhibit dissimilar virulence profiles, occur in separate geographical regions, and display distinct epidemiological characteristics and clinical manifestations [9]. *Trypanosoma brucei rhodesiense* causes an acute and rapidly progressing form of the disease, known as *rhodesiense* HAT (rHAT), which is localized to 13 countries in eastern and southern Africa [10]. It is a zoonotic disease [11], that is transmitted by tsetse flies of the *Glossina morsitans* group

[12] and passes directly or indirectly from animals or insects to humans. *Trypanosoma brucei gambiense* leads to a slow-progressing and chronic form of the disease, Gambian sleeping sickness or *gambiense* HAT (gHAT), which is found predominantly in 24 countries of western and central Africa [10]. The *palpalis* group is the vector of *T. b. gambiense*, with the main carriers being *Glossina palpalis palpalis* and *Glossina palpalis gambiensis* [13]. gHAT is an anthroponotic disease which is transmitted predominantly from person to person, although pigs and some wild animals have been reported as smaller reservoirs [11]. Infections from *T. b. gambiense* are the most common and represent over 97% of current cases [9].

Three severe outbreaks of the disease have been recorded in Africa. The first occurred between 1896 and 1906 with 800,000 deaths. The second began in 1920, peaking in 1930 with 70,000 registered cases, and ended in the late 1940s. The most recent widespread outbreak began in the 1970s and lasted until the end of the 1990s [14,15]. Incidence data from the World Health Organization (WHO) for 2009 showed a total of 9,878 new cases, with a sharp drop off observed in 2014. Nowadays, only the Democratic Republic of the Congo (DRC) reports an average of more than 1,000 new cases per year, comprising over 70% of the total recorded *T. b. gambiense* cases. However, the real number of people affected by this disease is estimated to be much higher due to under-reporting [8,16,17].

Tsetse flies are hematophagous, cyclical vectors of HAT [18]. Congenital transmission has also been demonstrated in newborn children within the first days of life and in older children born in nonendemic regions from infected mothers [19-22]. Transmission through sexual contact has been described once when the infection was passed from a male with confirmed gHAT to a woman who had never been to an endemic country [21-23]. Furthermore, mechanical transmission has also been reported *via* other blood-sucking insects, whereas accidental infections may occur from needle stick injuries in laboratories, or through blood transfusion [18,23].

HAT is clinically defined by two distinct stages. During the early hemolymphatic stage, trypanosomes spread and proliferate in the blood and the lymph. In the second or late meningoencephalitic stage, parasites are able to cross the blood-brain barrier (BBB) and invade the central nervous system (CNS) [16]. Although the progression of each stage involves different clinical features, it is often difficult to distinguish reliably between the two stages and they merge into each other, especially upon infection with *T. b. rhodesiense*. rHAT progresses rapidly and parasite invasion of the CNS occurs in a few weeks, causing death within months of infection. On the other hand, the neurological stage of gHAT generally starts several months or even years after infection, and the disease can take years or decades before becoming lethal [9,24].

After the bite from a tsetse fly, a chancre also known as a trypanome – a local skin reaction, develops at the feeding point. This occurs in about 20% of patients with rHAT, but is rarely observed in gHAT cases [10,11,25]. After an initial asymptomatic period that lasts one to three weeks in *rhodesiense*

infection, and usually some weeks longer in gHAT, patients develop nonspecific symptoms such as fever with chills, fatigue, headache, arthralgia, weight loss and a general sense of discomfort and unease. Splenomegaly, or less frequently hepatomegaly, has been observed, while enlargement of the posterior cervical lymph nodes, known as Winterbottom's sign, is common in Gambian sleeping sickness [10,11,16]. The meningoencephalitic stage involves symptoms from almost all regions of the nervous system. These clinical manifestations are categorized by psychiatric, motor, sensory disturbances and sleep abnormalities, the main features that gave the disease its name. Deep and painful hyperesthesia is the leading sensory symptom, known as Kerandel's sign. The disease causes deregulation of the circadian clock characterized by daytime somnolence followed by nocturnal insomnia. As the disease progresses, patients display an uncontrollable desire to sleep and alterations of sleep structure. During the final stage, cerebral edema, coma and systemic organ failure are observed, leading to sudden death [10,11,16,26-28].

The first issue in HAT diagnosis is to identify the disease as soon as possible by confirming the presence of parasites in the peripheral blood, or in other infected tissues such as the lymph nodes. Subsequently, the key step constitutes the accurate staging of the disease [29]. The non-specific signs and symptoms are insufficient for an accurate diagnosis. In rHAT, identification of trypanosomes is feasible because of the high levels of parasitemia, by microscopic examination of blood, or by a lymph node aspirate. The presence of the trypanosomal chancre is also typical of infection with *T. b. rhodesiense*. In contrast, *gambiense* infection is typified by cyclical parasitemia, reflecting a process of antigenic variation by the parasite, and parasitological diagnosis has poor sensitivity [7,24]. However, rapid and reliable serological tests (e.g., Card Agglutination Test for Trypanosomiasis (CATT), HAT Sero-K-SeT, SD Bioline HAT), based on the detection of specific antibodies, can be used for mass population screening [16,30,31]. Identification of the late stage of both types of HAT is based on the examination of cerebrospinal fluid (CSF) collected by lumbar puncture. WHO has defined 5 white blood cells (WBC) per μL as a threshold, or the presence of trypanosomes in the CSF, or both, as indicators that the infection has progressed to the CNS-stage. In *gambiense* infections, 20 cells per μL is used as the cutoff point [30]. Concentrations of immunoglobulin M (IgM) in the CSF, neopterin and combined panels of cytokines and chemokines, released after the tissue damage, have also been evaluated as biomarkers of HAT, and they reflect the severity of neurological signs [32,33].

Recognition of the causative *T. brucei* sub-species and correct staging of the disease are critical for choosing the appropriate chemotherapeutic regimen [10,34]. Drugs used for the first-stage disease are not able to cure second-stage disease, since therapy against the late stage requires drugs that travel across the BBB. Treatment of the first stage of sleeping sickness is limited to two drugs, pentamidine and suramin [35].

Pentamidine isethionate (Fig. (**1**)) is an aromatic diamidine and was registered as the drug of choice for the treatment of infection caused by *T. b. gambiense* in 1940. As a positively charged molecule, pentamidine interacts electrostatically with cellular polyanions. The drug seems to bind to the minor groove of DNA and to be involved in the disruption of both kinetoplast (kDNA) and nuclear DNA. kDNA is thought to be the primary target with drug activity linked to inhibition of the mitochondrial topoisomerase II. It has also been suggested that diamidines may act through other mechanisms, such as inhibition of the enzyme *S*-adenosylmethionine decarboxylase (AdoMetDC), or by deregulation of oxidative phosphorylation. [34,36-40].

Suramin (Fig. (**1**)) is a polysulphonated naphthylamine and has been used as a standard treatment for the hemolymphatic stage of rHAT. Suramin appears to bind to glycolytic enzymes through electrostatic interactions and inhibit them, thus interrupting glycolysis. In a recent study, dysregulation in cytokinesis was observed following suramin treatment, while parasites with more than two nuclei were abundant, indicating a possible new mode of action. Anaphylactic shock, renal failure, skin lesions, neurological complications, such as peripheral neuropathy, and bone marrow toxicity have been reported as the main adverse reactions [34,36,37,39,40].

Melarsoprol (Fig. (**1**)) is a trivalent arsenical and the only effective drug for the second stage of both forms of sleeping sickness. It was first used in 1949. Melarsoprol is a prodrug which is converted, in trypanosomes, into the active form melarsen oxide. The active metabolite seems to engage in stable interactions with sulfhydryl groups and has a high affinity for thiols such as trypanothione, affecting the redox (reduction–oxidation) balance of the parasites. It also interacts with a variety of glycolytic and pentose phosphate pathway enzymes, and thus, inhibits ATP synthesis. The use of melarsoprol is linked with a high frequency of severe and life-threatening adverse effects, with an overall mortality rate of 5%. This drug is very toxic, and patients may develop a severe post-treatment reactive encephalopathy (PTRE) with mortality rates that climb to 50%. [9,34,36,37,39,40].

Eflornithine (Fig. (**1**)) was originally registered as an anticancer drug, but in the 1980s, it was found to be an effective therapeutic solution for the second stage of gHAT. It is a specific and irreversible inhibitor of ornithine decarboxylase (ODC), the first enzyme involved in the biosynthesis of polyamines, which are essential for cell growth and proliferation. The main adverse effects reported are fever, pruritus, hypertension, bone marrow suppression, gastrointestinal symptoms and rarely, seizures. [34,36,37,39,40].

Combination regimens of melarsoprol, eflornithine and nifurtimox were assessed for the treatment of HAT. Nifurtimox is registered to treat patients with American trypanosomiasis (below). Nifurtimox-eflornithine combination therapy (NECT) (Fig. (**1**)) was found to be the most effective and now constitutes the first-line therapy for the late stage of *gambiense* infection. Nifurtimox is a prodrug that

is bioactivated through reduction of the nitro group, yielding nitro-anion radicals and other active metabolites. NECT is based on the synergistic actions of the two drugs; nifurtimox leads to oxidative stress and widespread damage to macromolecules, while eflornithine reduces the levels of trypanothione, the key redox-protecting metabolite. ~~Administration includes oral nifurtimox with a daily dose of 15 mg/kg, three times a day for 10 days, and eflornithine infusions of 400 mg/kg per day given every 12 hours for 7 days.~~ NECT produced a marked improvement in terms of administration (56 infusions reduced to 14), high cure rates, low mortality rates and less adverse side effects, especially compared to melarsoprol. Shorter hospitalization is also required, and the cost of the therapeutic schedule has been significantly reduced. ~~NECT-treated patients may be affected by musculoskeletal and abdominal pain, tremors, vomiting and nausea, headache and gastrointestinal disorders~~ [36,41-43].

Two new drugs are currently undergoing clinical trials, fexinidazole and acoziborole (Fig. (**1**)). Fexinidazole is a prodrug that is rapidly metabolized *in vivo* ~~through two different pathways, cytochrome P450 and a monooxygenase~~ into two metabolites, a sulfoxide and a sulfone, both of which exhibit trypanocidal activity. It is the only orally administered drug that is effective against both stages of HAT caused by *T. b. gambiense* and *T. b. rhodesiense.* ~~This drug has been deemed broadly acceptable due to the easy administration (one oral dose per day for 10 days), its safety profile, its reduced cost in terms of synthesis, and the fact that there is no requirement for disease staging.~~ Fexinidazole has received marketing authorization in the DCR for the treatment of gHAT, and has successfully entered phase 3 and phase 2 clinical trials in patients infected with gHAT of any stage and chronic Chagas disease, respectively [44-47].

Acoziborole (SCYX-7158) is another oral drug candidate that has been tested as a treatment for *T. b. gambiense* and *T. b. rhodesiense* infections. After phase 1 clinical trial, completed in 2015, it was confirmed that the drug is able to access the CNS, so may have potential against both disease stages. Phase IIb/III clinical trials have been ongoing in the DCR since 2016 [46-48].

~~A series of amidine-containing compounds have also been studied for their effect on *T. brucei* and some of them were evaluated in animal models and/or in clinical trials. However, the trials were discontinued due to high toxicity.~~
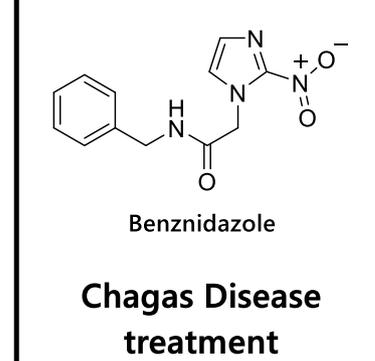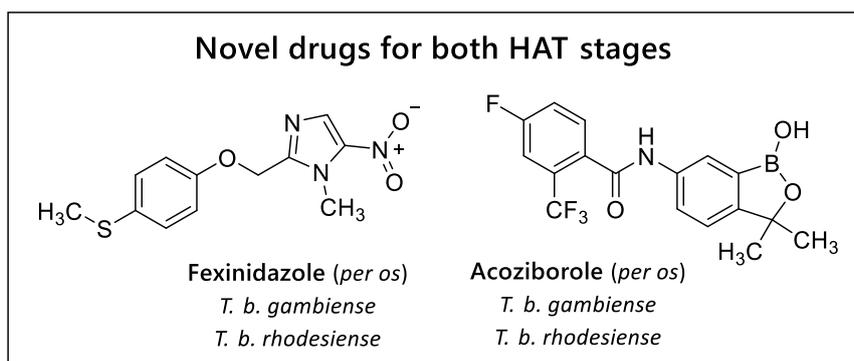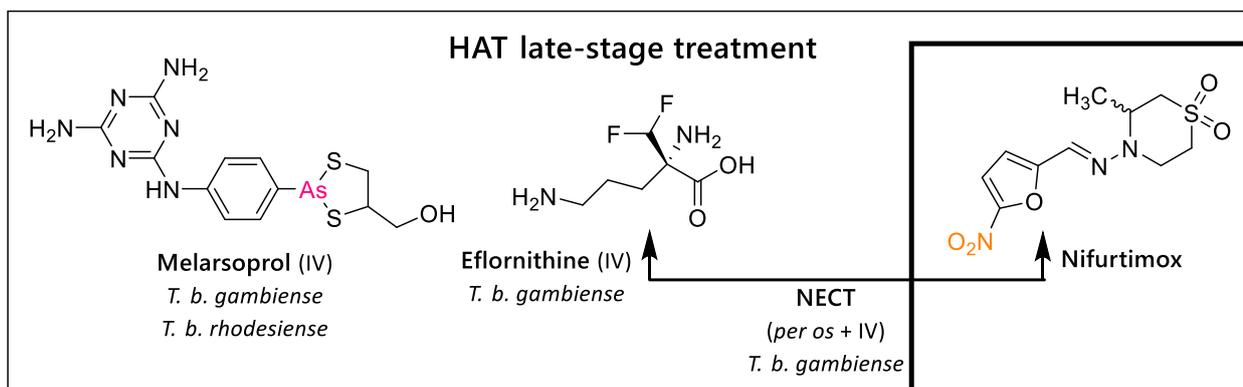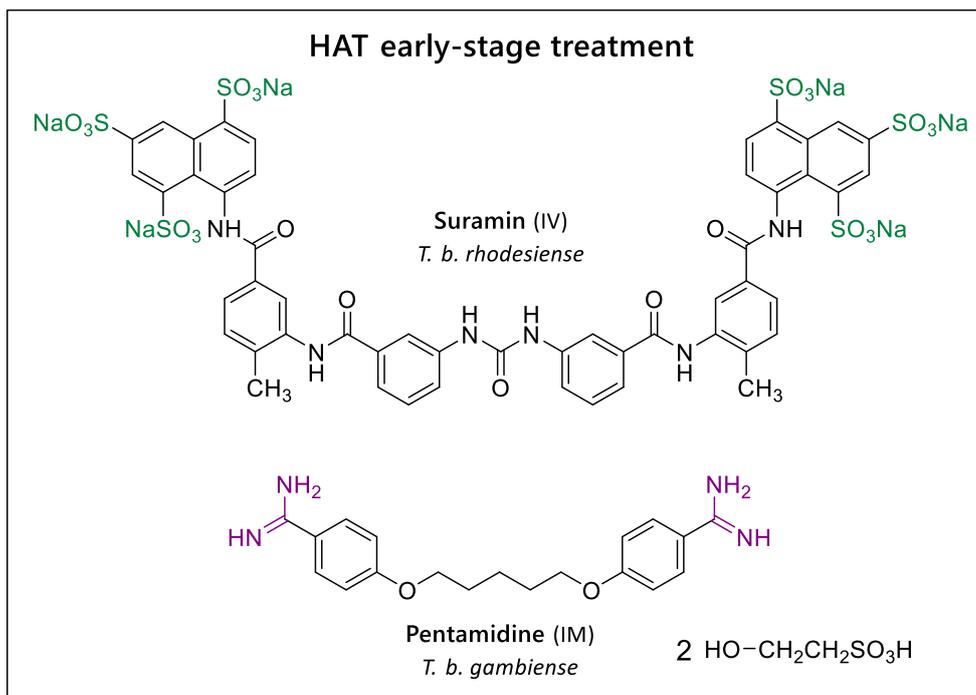
Fig. (1). Chemotherapeutic strategy against sleeping sickness and Chagas disease. Highlighted regions are reported to play a major role in the mechanism of action.

1.2 American trypanosomiasis

Chagas disease, or American trypanosomiasis, is a systemic, life-threatening zoonotic infection [49], caused by the protozoan parasite *Trypanosoma cruzi*. The disease is endemic in 21 ~~continental~~ Latin American countries, with an estimated 6-8 million people infected, mainly in poor rural areas, resulting in over 10,000 deaths annually. Chagas disease is also becoming a global public health problem. The migration of chronically infected individuals has spread the disease beyond its natural geographical boundaries, particularly to the USA and Europe [50]. The main route of transmission to humans is *via* the blood-sucking insect vector. Infection begins after mucous membranes, conjunctivae, or breaks in the skin become contaminated with parasites contained in the faeces of various species of the triatomine bug. However, other routes of transmission also exist; these include blood transfusion, organ transplantation, and vertical transmission from mother to infant [51,52]. Numerous outbreaks of the disease related to oral transmission, *via* food or liquid products contaminated with *T. cruzi*, have also been reported [49]. *T. cruzi* is able to invade almost all nucleated mammalian cells and has a wide host range.

Progression of the disease is characterized by two distinct clinical phases: an acute phase, and a chronic phase that develops over many years. The acute phase has a duration of 4-8 weeks and occurs shortly after the initial infection. This first stage is asymptomatic in 60 to 70% of patients. In the others, symptoms include inflammation at the inoculation site, fever, enlarged lymph nodes, splenomegaly and the highly characteristic unilateral palpebral oedema (Romaña sign). The infection is considered to be life-long, with 30% to 40% of patients subsequently developing chronic stage pathology, often 20 to 30 years after the acute infection. Symptoms can include cardiac disorders, mainly cardiomyopathy and arrhythmias, as well as gastrointestinal and/or neurological alterations that can result in death [51,53].

Currently, two drugs are available for the treatment of Chagas disease; nifurtimox (see above) and the most commonly used, benznidazole (BZ) (Fig. (**1**)). Recent findings suggest that BZ is responsible for the induction of potentially lethal double-stranded breaks in parasite DNA. This mechanism of action is based on reactive metabolites that are generated following nitroreductase mediated drug activation, which can damage DNA and other macromolecules, and result in the incorporation of oxidized nucleotides during DNA replication [54]. However, both drugs are only partially effective and relatively toxic, which, along with the prolonged administration required, limit their use [55].

There are no vaccines available against these two parasitic diseases. Vaccine development remains a daunting challenge, particularly in the case of HAT, where antigenic variation results in frequently changing surface glycoproteins that facilitate immune evasion. Thus, the major ways to prevent disease transmission are vector control and effective treatment. New and improved therapeutic options for both sleeping sickness and Chagas disease have been limited. The available drugs have

been in use for many years and are associated with poor efficacy, emergence of resistance, difficulties with administration, and severe adverse effects. Despite the progress made in the development of fexinidazole and, to a lesser extent, of acoziborole, both diseases continue to compromise public health in some of the poorest regions of the world. More efforts, focused on the discovery of new classes of therapeutics, are required [46,56,57].

1.3 The role of polyamines in trypanosomatids

The polyamine biosynthetic pathway is highly conserved across eukaryotic organisms and is crucial for the proliferation of trypanosomatids. The polyamines putrescine, spermidine and spermine are low molecular weight cationic organic amines that are essential for gene expression and cell growth, and play a crucial role in diverse cellular processes such as the biosynthesis of nucleic acids and proteins, cell proliferation and differentiation. The building blocks for the synthesis of polyamines (Fig. (**2**)) are the amino acids arginine and methionine. L-arginine is the substrate for the formation of L-ornithine, an intermediate of the urea cycle, upon hydrolysis catalyzed by arginase. L-ornithine is further decarboxylated to the diamine putrescine by ODC, the main regulatory enzyme in this pathway. *S*-adenosylmethionine synthase (AdoMet synthase) mediates the formation of *S*-adenosylmethionine (AdoMet) from methionine and ATP. Then, *S*-adenosylmethionine decarboxylase (AdoMetDC), a pyruvoyl-dependent enzyme, catalyzes the decarboxylation of AdoMet to generate an essential precursor (dcAdoMet) for spermidine biosynthesis. Subsequently, spermidine synthase transfers an aminopropyl group donated by the decarboxylated AdoMet to putrescine, forming spermidine. In mammalian cells and *T. cruzi*, addition of a second aminopropyl moiety leads to the synthesis of spermine *via* spermine synthase. Unique to trypanosomatid organisms, trypanothione, an essential redox cofactor, is required for defense against oxidative damage. Synthesis of this thiol is initiated by glutathionylspermidine synthase, which conjugates one glutathione molecule to spermidine, forming N1-glutathionylspermidine (Gsp). In the next step, a second glutathione is added to Gsp by trypanothione synthase, to generate trypanothione [58-60].
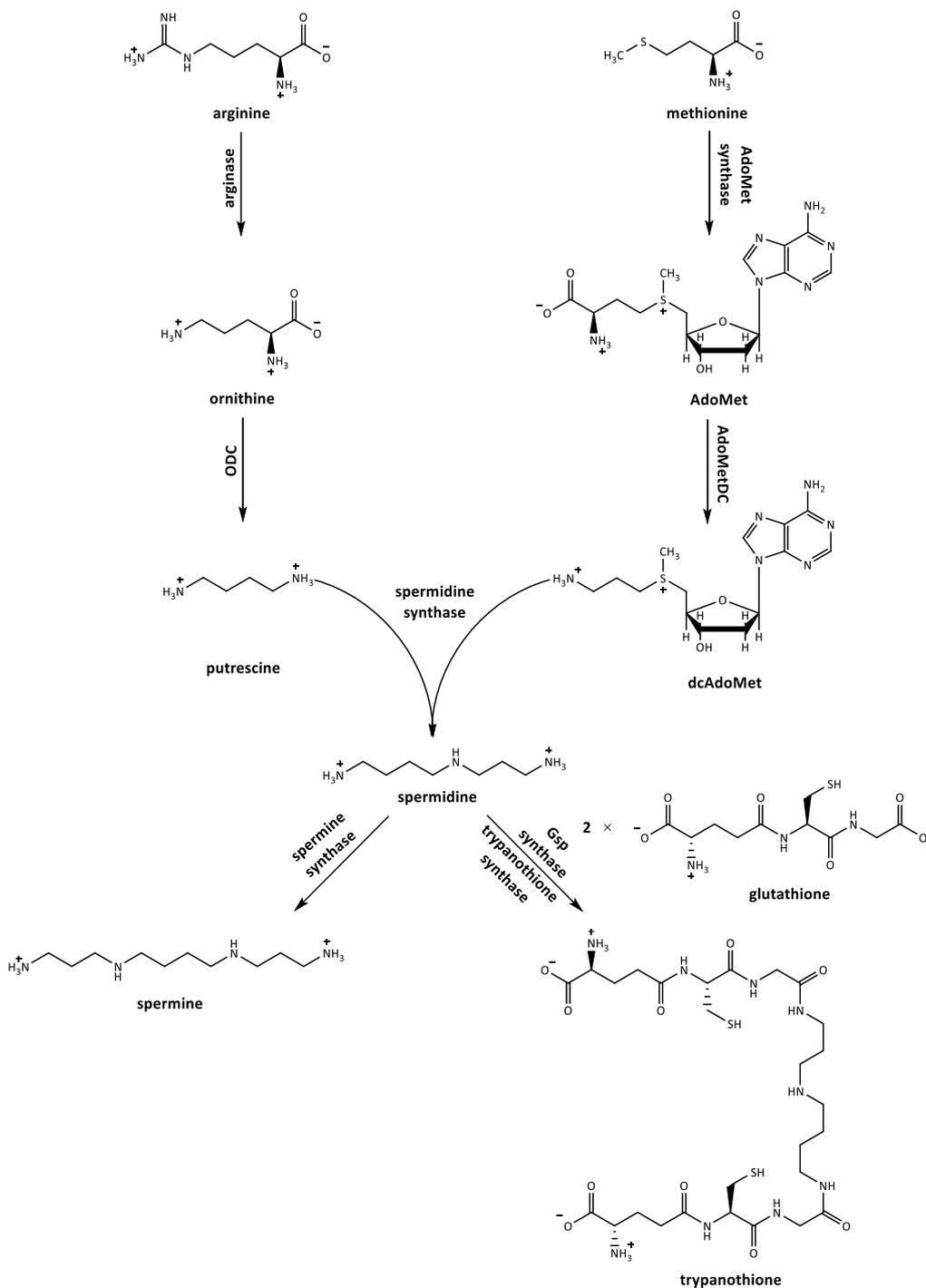
Fig. (2). Polyamine and trypanothione biosynthetic pathway.

In general, the enzymes involved in polyamine biosynthesis differ between mammalian cells and parasites in terms of their structural features, or their presence or absence from the host. Therefore, they emerge as potential targets for the development of trypanocidal agents. Of these enzymes, ODC and AdoMetDC, which regulate polyamine homeostasis, constitute druggable targets [61-63]. As previously described, ODC is inhibited irreversibly by eflornithine, and other approaches toward the inhibition of ODC in *T. brucei* are being considered. *T. cruzi* lacks this enzyme [64]. However, both

parasites do express AdoMetDC. Inhibitors of AdoMetDC have been reported that have potent activity against *T. brucei* and *T. cruzi in vitro*, as well as in mouse models [65-71]. The trypanosomatid AdoMetDC differs from the respective human enzyme, as it possesses a unique regulatory mechanism. The enzyme is allosterically activated by formation of a heterodimer between the active subunit and a catalytically inactive paralogous pseudoenzyme, referred to as a prozyme. Heterodimerization increases enzyme activity by three orders of magnitude. This novel regulation of the polyamine pathway in trypanosomatids suggests that selective inhibition of *T. brucei* AdoMetDC may be feasible, supporting the value of the target to combat HAT [72].

1.4 Drug design

Adamantane

The adamantane scaffold is a polycyclic cage moiety, characterized by high symmetry and a unique geometry of three fused cyclohexanes in a chair-like conformation. It is a rigid and practically strain-free structure that has been applied as a valuable structural subunit in medicinal chemistry for many years [73]. The adamantane moiety can either be incorporated into existing drugs to improve their pharmacokinetic and pharmacodynamic profile, or used as a starting compound for the development of novel therapeutic agents. ~~Therefore, it has been widely used in drug discovery strategies.~~ More specifically, it has been demonstrated that the addition of the adamantyl moiety into a molecule enhances its overall lipophilicity and subsequently increases cell membrane permeability of the drug candidate [73-75]. Another example of adamantane's usefulness ~~in medicinal chemistry~~ is the increased affinity for lipophilic receptors that it confers, presumably due to greater hydrophobic interactions, giving rise to higher selectivity. Adamantane can be used to add steric bulk to a compound and to protect nearby functional groups from metabolic cleavage, thus offering greater stability and prolonged duration of action [73,75,76]. Finally, ~~due to its rigidity and bulkiness,~~ this cage scaffold can accommodate *β*-cyclodextrins (*β*-CD), resulting in inclusion complexes, or act mechanically as a blocker for several ion channels [77,78]. ~~Because of all the above, the adamantyl subunit constitutes a privileged building block that provides drug-like properties to lead compounds.~~ Amantadine, rimantadine, memantine, tromantadine, adapalene, vildagliptin and saxagliptin are seven examples of adamantane-containing marketed drugs (Fig. (**3**)) that are available today. Currently approved uses for the above-mentioned therapeutics range from viral infections (Influenza A, *Herpes simplex*), and neurodegenerative disorders (Parkinson's disease, Alzheimer's disease), to acne vulgaris and type II diabetes mellitus. It therefore comes as no surprise that many adamantyl compounds are under development, yielding a plethora of pharmacologically active analogues that

have been studied for various medical conditions, including iron overload disease, cancer, CNS diseases, inflammation, hypertension, hyperglycemia, malaria and tuberculosis [74-76,78-81].
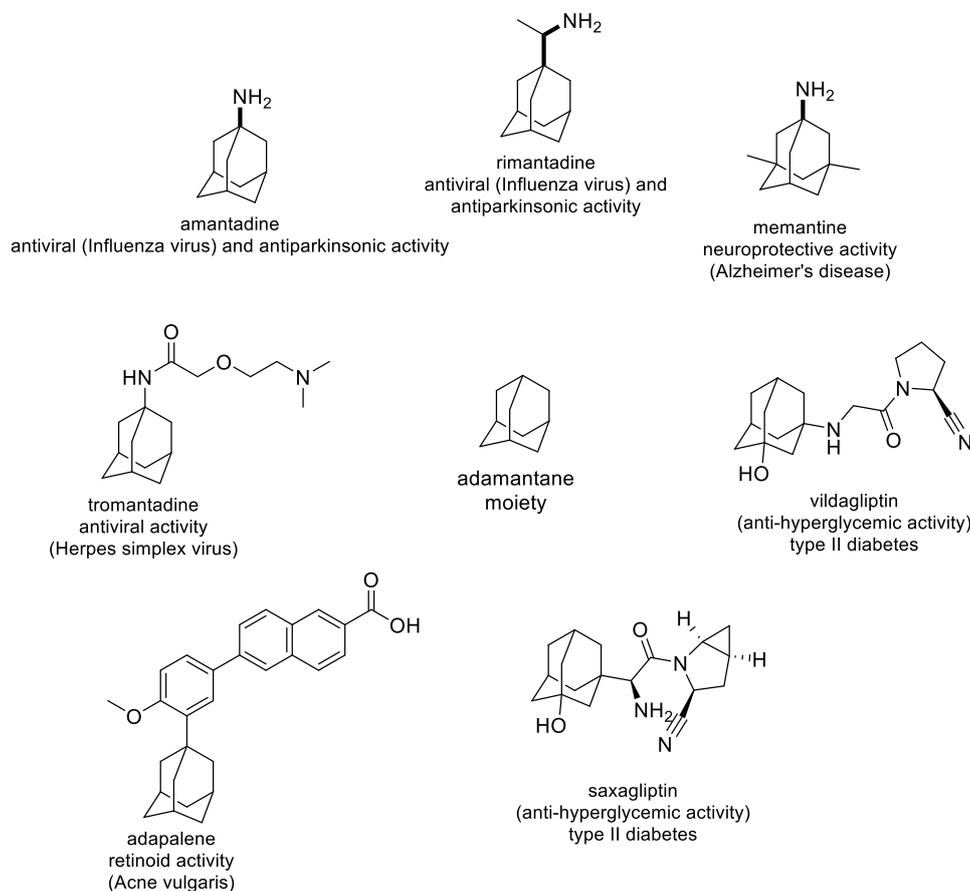

Fig. (3). Clinically approved adamantane derivatives and their pharmacological profiles.

Adamantane-based guanylhydrazone analogues

Over the years, we have synthesized a variety of structurally diverse adamantane derivatives that target influenza A virus, *T. brucei* and *T. cruzi* [96-103]. In continuation of our studies, we were interested in developing further active adamantane-based compounds that could inhibit the proliferation of the above-mentioned trypanosomatids. Intrigued by the *in vitro* and *in vivo* trypanocidal properties of several guanylhydrazone analogues, that could act as potential AdoMetDC inhibitors [104-112], and following a molecular hybridization approach, we designed derivatives of the adamantane core bearing the iminoguanidine moiety in position 2 of the cage (Fig. (**4**)) [113].

Series 1

G_1 R_1 = H, R_2 = H, R_3 = H, R_4 = H
G_2 R_1 = H, R_2 = NNHC(=NH)NH$_2$ · HCl, R_3 = H, R_4 = H
G_3 R_1 = H, R_2 = H, R_3 = H, R_4 = NNHC(=NH)NH$_2$ · HCl
G_4 R_1 = H, R_2 = OH, R_3 = H, R_4 = H, racemic
G_5 R_1 = H, R_2 = H, R_3 = OH, R_4 = H

Series 2

G_6 R = C_4H_9, n = 2, X = NH
G_7 R = C_6H_{13}, n = 2, X = NH
G_8 R = C_8H_{17}, n = 2, X = NH
G_9 R = $C_{12}H_{25}$, n = 2, X = NH
G_{10} R = C_4H_9, n = 2, X = S
G_{11} R = $C_{12}H_{25}$, n = 2, X = S

G_{12} R = C_6H_{13}, n = 2
G_{13} R = C_7H_{15}, n = 2
G_{14} R = C_8H_{17}, n = 2
G_{15} R = $C_{10}H_{21}$, n = 2
G_{16} R = C_6H_{13}, n = 3
G_{19} R = PhCH$_2$, n = 1
G_{20} R = PhCH$_2$, n = 2
G_{21} R = PhCH$_2$, n = 3

G_{17} n = 2, m = 3
G_{18} n = 5, m = 0

Series 3

Series 4

G_{22} X = H, n = 0
G_{23} X = H, n = 1
G_{24} X = F, n = 1
G_{25} X = OCH$_3$, n = 1

Fig. (4). Structures of adamantane-substituted guanylhydrazones **G1** – **G25** ~~described in the present study~~ [112-114].

~~From this perspective~~, The design strategy was aimed at combining the increased lipophilicity of the adamantane cage structure with the trypanocidal properties ~~activity~~ of the guanylhydrazone moiety to generate compounds with better antiparasitic activity. The general approach ~~for this class of compounds~~ was to use the adamantane component as a lipid carrier for the BBB to counterbalance the potential transport limitations conferred by the conjugated polar iminoguanidine side chain. Thus, improving their BBB permeability enables enhanced CNS penetration and increased concentration in brain tissue, which is of crucial importance for the treatment of the second stage HAT. Finally, the incorporation of the guanylhydrazone group into this class of compounds should have the added advantage of structural similarity with the guanidine pharmacophore of the licensed trypanocidal drug pentamidine. To study the impact of changing the guanylhydrazone position and to evaluate the significance of the adamantane scaffold, we proceeded with the synthesis of novel guanylhydrazone derivatives (~~Series 5~~, Fig. (5)). In analogues **G26** and **G27,** the iminoguanidine group was shifted to the methylene carbon of the benzyl substituent, leading to ~~the idea of~~ synthesis of the fused adamantane-cyclopentane-benzene guanylhydrazone analogue **G28**. Finally, replacement of the

adamantane cage structure by the tricyclic scaffolds of fluorene and dibenzocycloheptene, and the bendable 4-phenyl cyclohexane, ~~afforded~~ led to ~~the~~ analogues **G29**, **G30** and **G31**, respectively.
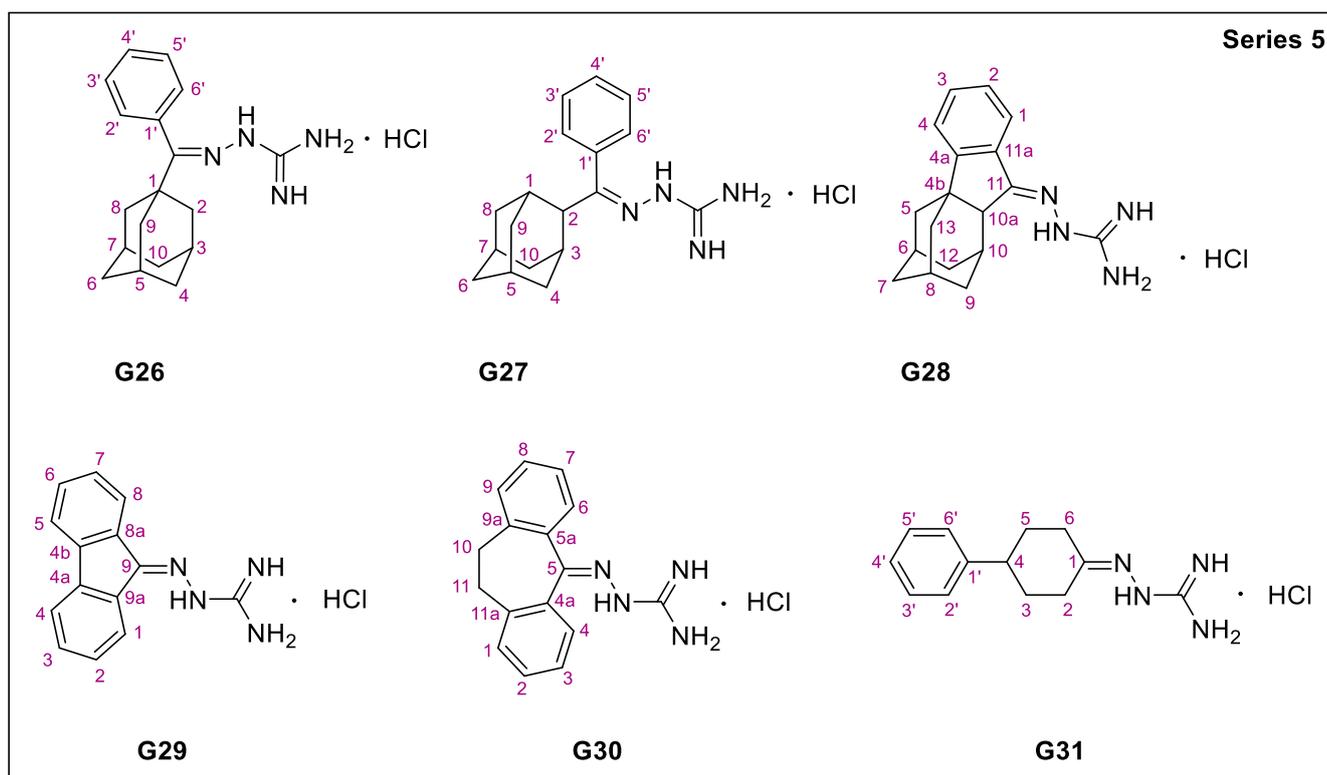

Fig. (5). Structures of novel guanylhydrazone derivatives **G26** – **G31**, ~~synthesized in the present study.~~

Here, we report the synthesis and structural characterization of novel guanylhydrazones (**G26** – **G31**, Fig. (**5**)), with their subsequent *in vitro* biological evaluation against bloodstream form *T. brucei* and *T. cruzi* epimastigotes. We also report, for the first time, the results of the trypanocidal activity of previously synthesized adamantane guanylhydrazones (**G1** – **G5**, Fig. (**4**)) that have been used as butyrylcholinesterase inhibitors. Finally, we provide an overview on the chemistry and pharmacological activity of adamantane-based guanylhydrazone derivatives (**G6** – **G25**, Fig. (**4**)), synthesized in the recent past, ~~by our research group~~. ~~Yet~~ Another objective of the study was to evaluate the effect of structural modifications and steric parameters on antiparasitic activity and to correlate this activity with possible interactions in the active site of AdoMetDC, using docking-scoring calculations and Quantitative Structure-Activity Relationship (QSAR) studies.

2. Experimental

2.1 General Experimental methods and techniques

Melting points were determined using a Büchi capillary apparatus and are uncorrected. NMR experiments were performed to elucidate the structure and determine the purity of the newly synthesized compounds. ^{1}H NMR and 2D NMR spectra (COSY, HSQC, HSQC-DEPT and HMBC) were recorded on a Bruker Ultrashield™ Plus Avance III 600 spectrometer (600.11 MHz, ^{1}H NMR). ^{13}C NMR spectra were recorded on a Bruker Ultrashield™ Plus Avance III 600 spectrometer (150.9 MHz, ^{13}C NMR). Chemical shifts δ *(delta)* are reported in parts per million (ppm) downfield from the NMR solvent, with the tetramethylsilane or solvent (DMSO-d_6) as internal standard. Data processing including Fourier transformation, baseline correction, phasing, peak peaking and integrations were performed using MestReNova software v.12.0.0. Splitting patterns are designated as follows: s, singlet; br s, broad singlet; d, doublet; t, triplet; q, quartet; dd, doublet of doublets; dt, doublet of triplets; dq, doublet of quartets; td, triplet of doublets; tt, triplet of triplets; ttd, triplet of triplets of doublets; qd, quartet of doublets; quin, quintet; complex m, complex multiplet. Coupling constants (J) are expressed in units of Hertz (Hz). The spectra were recorded at 305 K (32 °C) unless otherwise specified. The solvent used to obtain the spectra was deuterated dimethyl sulfoxide, DMSO-d_6 (quin, 2.50 ppm, ^{1}H NMR; septet, 39.52 ppm, ^{13}C NMR). Elemental analyses (C, H, N) were performed by the Service Central de Microanalyse at CNRS (France), and were within ± 0.4% of the theoretical values. Elemental analysis results for the tested compounds correspond to >95% purity. The commercial reagents were purchased from Alfa Aesar, Sigma-Aldrich, and Merck, and were used without further purification. Organic solvents used were of the highest purity.

2.2 Synthetic procedure for the preparation of analogues G26 – G31

Aminoguanidine bicarbonate (1.5 mmol) was suspended in 18 mL of absolute ethanol, and it was progressively dissolved by dropwise acidification with concentrated hydrochloric acid, until pH was adjusted to 2. Subsequently, the appropriate ketone (1.5 mmol) was added and the mixture was refluxed under stirring for 5 h at 105 – 110 °C. After completion of the reaction time, ethanol was evaporated under reduced pressure and the residue was treated with dry Et$_2$O. The resulting product was cooled at 5 °C for 1 h and filtered off *in vacuo*. The precipitate was washed with dry Et$_2$O and dried to obtain the desired analogues **G26 – G31** as crystals.

Tricyclo[3.3.1.1^{3,7}]decan-1-yl(phenyl)methylene)guanylhydrazone hydrochloride (G26)

Product **G26** was obtained using 500 mg (2.08 mmol) of 1-adamantyl phenyl ketone and 283 mg (2.08 mmol) aminoguanidine bicarbonate in 25 mL of absolute EtOH, resulting in 690 mg of white crystalline solid. Yield: almost quantitative; mp >250 °C (from EtOH/dry Et_2O); ^{1}H NMR (600.11 MHz, DMSO-d_6) δ (ppm) [1.57 (dq, 3H, J_1=12.2 Hz, J_2=2.1 Hz), 1.66 (dt, 3H, J_1=12.5 Hz, J_2=3.1 Hz), H_4-Ad, H_6-Ad, H_{10}-Ad], 1.75 (d, 3H, J=3.0 Hz, H_2-Ad, H_8-Ad, H_9-Ad), 1.96 (~quin, 3H, J=3.2 Hz, H_3-Ad, H_5-Ad, H_7-Ad), 7.09 (dd, 2H, J_1=8.1 Hz, J_2=1.5 Hz, $H_{2'}$, $H_{6'}$), 7.32-8.01 (br s, 3H, NHC(N*H*)N*H*$_2$), 7.47-7.54 (complex m, 3H, $H_{3'}$, $H_{4'}$, $H_{5'}$), 9.25 (s, 1H, N*H*C(NH)NH$_2$); ^{13}C NMR (150.9 MHz, DMSO-d_6) δ (ppm) 27.6 (C_3-Ad, C_5-Ad, C_7-Ad), 36.0 (C_4-Ad, C_6-Ad, C_{10}-Ad), 39.4 (C_2-Ad, C_8-Ad, C_9-Ad), 127.6 ($C_{2'}$, $C_{6'}$), 129.0 ($C_{3'}$, $C_{5'}$), 129.1 ($C_{4'}$), 131.3 ($C_{1'}$), 155.7 (NH*C*(NH)NH$_2$), 164.6 (*C*=N). Anal. calcd. For $C_{18}H_{25}ClN_4$, C, 64.95; H, 7.57; N, 16.83. Found: C, 65.00; H, 7.50; N, 16.79.

Tricyclo[3.3.1.1^{3,7}]decan-2-yl(phenyl)methylene)guanylhydrazone hydrochloride (G27)

Product **G27** was obtained using 500 mg (2.08 mmol) of 2-adamantyl phenyl ketone and 283 mg (2.08 mmol) aminoguanidine bicarbonate in 25 mL of absolute EtOH, resulting in 680 mg of white crystalline solid. Yield: almost quantitative; mp >250 °C (from EtOH/dry Et_2O); ^{1}H NMR (600.11 MHz, DMSO-d_6) δ (ppm) 1.45 (d, 2H, J=12.3 Hz, H_{4e}-Ad, H_{9e}-Ad), 1.66 (d, 2H, J=3.1 Hz, H_6-Ad), 1.69-1.78 (complex m, 4H, H_8-Ad, H_{10}-Ad), 1.79 (~quin, 1H, J=3.1 Hz, H_5-Ad), 1.86 (~quin, 1H, J=3.0 Hz, H_7-Ad), 1.93 (dd, 2H, J_1=12.8 Hz, J_2=2.8 Hz, H_{4a}-Ad, H_{9a}-Ad), 2.04 (q, 2H, J=2.9 Hz, H_1-Ad, H_3-Ad), 2.92 (s, 1H, H_2-Ad), 7.09-7.29 (br s, 3H, NHC(N*H*)N*H*$_2$), 7.28 (dd, 2H, J_1=8.2 Hz, J_2=1.4 Hz, $H_{2'}$, $H_{6'}$), 7.47 (td, 1H, J_1=7.4 Hz, J_2=1.4 Hz, $H_{4'}$), 7.51 (~dd, 2H, J_1=8.1, 6.6 Hz, J_2=1.5 Hz, $H_{3'}$, $H_{5'}$), 9.74 (s, 1H, N*H*C(NH)NH$_2$); ^{13}C NMR (150.9 MHz, DMSO-d_6) δ (ppm) 27.2 (C_5-Ad), 27.3 (C_7-Ad), 28.6 (C_1-Ad, C_3-Ad), 32.0 (C_4-Ad, C_9-Ad), 37.1 (C_6-Ad), 37.9 (C_8-Ad, C_{10}-Ad), 50.1 (C_2-Ad), 126.9 ($C_{2'}$, $C_{6'}$), 129.3 ($C_{3'}$, $C_{5'}$), 129.4 ($C_{4'}$), 155.8 (NH*C*(NH)NH$_2$), 159.5 (*C*=N). Anal. calcd. For $C_{18}H_{25}ClN_4$, C, 64.95; H, 7.57; N, 16.83. Found: C, 64.91; H, 7.63; N, 16.85.

Adamantane[1,2-a]inden-11-ylidene)guanylhydrazone hydrochloride (G28)

Product **G28** was obtained using 500 mg (2.10 mmol) of adamantane[1,2-a]inden-11-one and 286 mg (2.10 mmol) aminoguanidine bicarbonate in 25 mL of absolute EtOH, resulting in 575 mg of white crystalline solid. Yield: 83%; mp 230 – 232 °C (from EtOH/dry Et_2O); ^{1}H NMR (600.11 MHz, DMSO-d_6) δ (ppm) 1.51 (d, 2H, J=12.5 Hz, H_{9e}-Ad, H_{13e}-Ad), 1.61-2.08 (complex m, 7H, H_5, H_7, H_8, H_{12}), 2.31 (t, 4H, J=11.2 Hz, H_6, H_{9a}, H_{10}, H_{13a}), 2.81 (s, 1H, H_{10a}), 7.29 (t, 1H, J=7.2 Hz, H_3), 7.48 (t, 1H, J=7.4 Hz, H_2), 7.83 (d, 1H, J=7.7 Hz, H_1), 7.84-8.11 (br s, 3H, NHC(N*H*)N*H*$_2$), 8.22 (d, 1H, J=7.6 Hz, H_4), 10.33 (s, 1H, N*H*C(NH)NH$_2$); ^{13}C NMR (150.9 MHz, DMSO-d_6) δ (ppm) 27.0 (C_8), 27.1 (C_6), 27.6 (C_{10}), 32.2 (C_7), 36.3 (C_9), 36.5 (C_{12}), 42.3 (C_{4b}), 46.7 (C_{13}), 47.8 (C_5), 82.6

(C_{10a}), 122.2 (C_4), 126.0 (C_2), 128.0 (C_3), 133.8 (C_1), 136.1 (C_{4a}), 156.5 (C=N), 158.2 (NHC(=NH)NH$_2$), 162.5 (C_{11a}). Anal. calcd. For $C_{18}H_{23}ClN_4$, C, 65.34; H, 7.01; N, 16.93. Found: C, 65.40; H, 7.08; N, 16.88.

2-(9H-Fluoren-9-ylidene)guanylhydrazone hydrochloride (G29)

Product **G29** was obtained using 500 mg (2.77 mmol) of 9H-fluoren-9-one and 377 mg (2.77 mmol) aminoguanidine bicarbonate in 33 mL of absolute EtOH, resulting in 695 mg of yellow crystalline solid. Yield: 92%; mp 238 – 240 °C (from EtOH/dry Et$_2$O); ^{1}H NMR (600.11 MHz, DMSO-d_6) δ (ppm) [7.35 (td, 1H, J_1=7.4 Hz, J_2=0.9 Hz), 7.39 (td, 1H, J_1=7.6 Hz, J_2=1.2 Hz), H$_2$, H$_7$], [7.44 (td, 1H, J_1=7.5 Hz, J_2=1.2 Hz), 7.54 (t, 1H, J=7.5 Hz), H$_3$, H$_6$], [7.79 (d, 1H, J=7.5 Hz), 7.88 (d, 1H, J=7.5 Hz), H$_4$, H$_5$], 8.11 [(d, 1H, J=7.5 Hz), 8.76 (d, 1H, J=7.7 Hz), H$_1$, H$_8$], 8.23-8.67 (br s, 3H, NHC(NH)NH_2), 11.45 (s, 1H, NHC(NH)NH$_2$); ^{13}C NMR (150.9 MHz, DMSO-d_6) δ (ppm) 120.2, 120.9 (C_4, C_5), 122.7, 127.4 (C_1, C_8), 128.2, 128.3 (C_2, C_7), 130.7, 131.9 (C_3, C_6), 136.3, 139.1 (C_{8a}/C_{9a}), 141.8 (C_{4a}, C_{4b}), 148.2 (C=N), 157.3 (NHC(=NH)NH$_2$). Anal. calcd. For $C_{14}H_{13}ClN_4$, C, 61.65; H, 4.80; N, 20.54. Found: C, 61.70; H, 4.89; N, 20.49.

2-(10,11-Dihydro-5H-dibenzo[a,d][7]annulen-5-ylidene)guanylhydrazone hydrochloride (G30)

Product **G30** was obtained using 1.0 g (4.80 mmol) of 10,11-dihydro-5H-dibenzo[a,d][7]annulen-5-one (dibenzosuberone) and 653 mg (4.80 mmol) aminoguanidine bicarbonate in 58 mL of absolute EtOH, resulting in 405 mg of beige crystalline solid. Yield: 28%; mp 155-157 °C (from EtOH/dry Et$_2$O); ^{1}H NMR (600.11 MHz, DMSO-d_6) δ (ppm) [2.87 (dd, 2H, J_1=17.8 Hz, J_2=10.0 Hz), 3.06 (d, 1H, J=13.6 Hz), 3.26 (d, 1H, J=17.2 Hz), H$_{10}$, H$_{11}$], 7.13 (d, 1H, J=7.7 Hz, H$_1$ or H$_9$), [7.22 (t, 1H, J=7.4 Hz), 7.23 (t, 1H, J=7.1 Hz), H$_3$, H$_7$], 7.29 (d, 1H, J=7.4 Hz, H$_4$ or H$_6$), 7.33 (t, 1H, J=7.3 Hz, H$_2$ or H$_8$), 7.41 (d, 1H, J=7.3 Hz, H$_1$ or H$_9$), 7.43 (t, 1H, J=7.8 Hz, H$_2$or H$_8$), 7.55-8.13 (br s, 3H, NHC(NH)NH_2), 7.75 (d, 1H, J=7.7 Hz, H$_4$/H$_6$), 10.13 (s, 1H, NHC(NH)NH$_2$); ^{13}C NMR (150.9 MHz, DMSO-d_6) δ (ppm) 31.1, 33.5 (C_{10}, C_{11}), 126.1, 126.6 (C_3, C_7), 127.3, 128.8 (C_2, C_8), 129.3, 129.6 (C_4, C_6), 130.6, 130.8 (C_1, C_9), 133.4, 135.2 (C_{4a}, C_{5a}), 138.4, 139.4 (C_{9a}, C_{11a}), 156.2 (C=N), 159.1 (NHC(=NH)NH$_2$). Anal. calcd. For $C_{16}H_{17}ClN_4$, C, 63.89; H, 5.70; N, 18.63. Found: C, 63.93; H, 5.82; N, 18.66.

2-(4-Phenylcyclohexylidene)guanylhydrazone hydrochloride (G31)

Product **G31** was obtained using 500 mg (2.87 mmol) of 4-phenylcyclohexan-1-one and 391 mg (2.87 mmol) aminoguanidine bicarbonate in 34 mL of absolute EtOH, resulting in 760 mg of white crystalline solid. Yield: almost quantitative; mp 218 – 220 °C (from EtOH/dry Et$_2$O); ^{1}H NMR (600.11 MHz, DMSO-d_6) δ (ppm) 1.59 (qd, 1H, J_1=12.9 Hz, J_2=4.1 Hz, H$_{2a}$ or H$_{6a}$), 1.64 (qd, 1H,

J_1=12.7 Hz, J_2=4.3 Hz, H3a or H5e), 1.98 (~ttd, 2H, J_1=9.3 Hz, J_2=6.3, 5.8 Hz, J_3=3.3 Hz, H2a or H6a, H3a or H5e), 2.14 (td, 1H, J_1=14.1 Hz, J_2=5.1 Hz, H2e or H6e), 2.42 (td, 1H, J_1=13.5 Hz, J_2=4.8 Hz, H3e or H5a), 2.50-2.55 (m, 1H, H3e or H5a), 2.85 (tt, 1H, J_1=12.2 Hz, J_2=3.5 Hz, H4), 3.15 (dq, 1H, J_1=14.7 Hz, J_2=3.0 Hz, H2e or H6e), 7.25 (d, 2H, J=7.4 Hz, H2', H6'), 7.28 (t, 2H, J=7.5 Hz, H3', H5'), 7.48-7.95 (br s, 3H, NHC(=N*H*)N*H$_2$*), 8.84 (s, 0.25H, N*H*C(=NH)NH$_2$) 11.34 (s, 0.75H, N*H*C(=NH)NH$_2$); ^{13}C NMR (150.9 MHz, DMSO-d_6) δ (ppm) 27.3, 32.5 (C_2, C_6), 33.8, 34.3 (C_3, C_5), 42.2 (C_4), 126.1 ($C_{4'}$), 126.6 ($C_{2'}$, $C_{6'}$), 128.3 ($C_{3'}$, $C_{5'}$), 145.5 ($C_{1'}$), 156.2 (NH*C*(=NH)NH$_2$), 158.8 (*C*=N), 159.2 (*C*=N). Anal. calcd. For $C_{13}H_{19}ClN_4$, C, 58.53; H, 7.18; N, 21.00. Found: C, 58.50; H, 7.25; N, 21.07.

2.3 Trypanocidal assays

For compounds **G1** – **G25**: A bloodstream form of *T. brucei* ~~brucei~~ (strain 427, derivative 221) was cultured in 25 mL flasks at 37 °C in modified Iscove's medium (pH 7.4) [115]. To assess activity, parasites were grown for 3 days in the presence of test compounds and the EC_{50} and EC_{90} values were determined (concentrations that inhibit growth by 50% and 90%, respectively). In these experiments, the densities of untreated cultures increased from 0.25×10^4 to 4×10^6 cells mL^{-1}. After determination of cell densities at each drug concentration with a hemocytometer (Weber Scientific International Ltd.), drug sensitivity was expressed as a percentage of growth of control cells. Data presented are the mean of triplicate experiments ± SEM.

For compounds **G26** – **G31**: Bloodstream form *T. brucei* (strain 427, derivative 221) were cultured in modified Iscove's medium, as outlined previously [116]. Eight-point potency curves were performed in 96-well plates (200 μL volumes), and the compound concentrations that inhibited growth by 50% (EC_{50}) and 90% (EC_{90}) were determined. Parasites were first diluted to 2.5×10^4 mL^{-1}, compounds were added at range of concentrations, and the plates incubated at 37 °C. Resazurin was added after 48 h, and the plates incubated for a further 16 h. *T. cruzi* epimastigotes (strain CL Brener) were cultured as previously described [117]. Trypanocidal activity was determined in microtiter plates as outlined above, with the following modifications. Experiments were initiated by seeding the parasites at 2.5×10^5 mL^{-1}, and after the addition of test compounds, cultured at 28 °C for 4 days. Resazurin was added, the plates were incubated for a further 2 days, and then assessed as above. Fluorescence intensities were determined using a BMG FLUOstar Omega (excitation 545 nm, emission 590 nm). Data were analyzed using Graph Pad Prism 7 software. Values are expressed as EC_{50} ± SD and are the average of three independent replicates.

2.4 *In vitro* cytotoxicity assays on rat skeletal myoblast L6 cells

Cytotoxicity against L6 cells was assessed using microtiter plates. Briefly, cells were seeded in triplicate at 1×10^4 mL^{-1} in growth medium containing different compound concentrations. The plates were incubated for 6 days at 37 °C and resazurin was then added to each well. After a further 8 h of incubation, the fluorescence was determined using a BMG FLUOstar Omega plate reader.

2.5 Computer-aided drug design

The discovery of new drugs is ~~undoubtedly~~ an expensive and time-consuming multi-step process. However, it is accelerated through our increased understanding of the fundamental principles of protein-ligand interactions, in addition to the integration of a computer-aided drug design (CADD) strategy. CADD strategies involve application of computer modelling technologies, which ultimately aid in selection and filtering of candidate compounds, generation of hypotheses on ~~their~~ mode of action, and ~~also~~ facilitate their further development [118,119]. Over the last decades, due to advancements in computer technology, CADD has been considered a rapidly growing field and plays a crucial role in drug development projects, from hit identification to lead optimization of novel, potentially therapeutically valuable small molecules [120-123]. CADD strategies can be mainly classified into three broad categories; the ligand-based (LBDD) and the structure-based (SBDD) approaches, as well as fragment-based drug discovery (FBDD), a newly emerging lead discovery method [124,125]. LBDD approaches utilize structure and activity data from a set of known active and inactive compounds in order to retrieve other potential molecular scaffolds based on similarity measures, common pharmacophores or descriptor values. LBDD methods include, amongst others, similarity and substructure searching, quantitative structure-activity relationships (QSAR), as well as pharmacophore and three-dimensional (3D) shape matching [126,127]. Contrarily, SBDD approaches are based on direct calculation of protein-ligand interactions utilizing the 3D structure of the biological target, determined through X-ray crystallography and NMR, or through homology modeling, and include ligand docking-based scoring, molecular dynamics and *de novo* design [128]. Notably, both of the above mentioned knowledge-driven approaches can be synergistically integrated to improve the drug design process [129]. In this current study, we are mainly focusing on QSAR analysis *via* 2D fingerprint similarity and docking-based scoring, one methodology from each CADD approach.

2.6 Docking-based scoring

Introduction

The docking process involves the prediction of ligand conformation and posing, as well as binding interactions within the targeted protein site. This is a rather challenging task by itself, since even relatively simple organic molecules may contain many conformational degrees of freedom, or show a diversity of binding modes. Thorough sampling of ligand orientation within the binding domain of the target is provided through stochastic search techniques such as the Monte Carlo algorithm [130]. Rapid and accurate assessment of protein-ligand complexes is pivotal for docking approaches, since a typical ligand docking experiment generates hundreds to thousands of ligand conformations [131]. Thus, an efficient scoring function is essential to rank order different docked poses for each ligand, and ultimately to discriminate the valid binding mode predictions from the invalid ones [132]. Evaluation of docked poses is achieved by four distinct classes of scoring functions that are currently applied in computational drug design: force-field-based, empirical, knowledge-based and a rather new approach, machine learning-based scoring functions [133], with the first being the scoring function of our choice.

Protocol

Prior to any docking experiment, protein and ligand databases need to be prepared. The crystal structure of *T. brucei* AdoMetDC/prozyme heterodimer (PDB structure: 5tvf) was computationally cleaved to include only AdoMetDC in complex with the bound ligand, CGP. Then, Protein Preparation Wizard [134] workflow was executed, as ~~previously thoroughly~~ described in detail previously [135], generating a structurally sound model ensuring accuracy on all downstream modeling simulations. Preparation of the guanylhydrazone analogues was performed using the LigPrep tool [136]. LigPrep generates precise, energy minimized 3D molecular structures with correct protonation states, tautomerism and enumeration of all possible stereoisomers. Docking grid preparations and docking calculations were accomplished as previously described [135]. Two different grids were generated using no scaling for protein van der Waals (VdW) radii and an extended ligand centering box of $10 \times 10 \times 10$ Å and $15 \times 15 \times 15$ Å, respectively, to ensure proper fitting of the large aliphatic chains of some guanylhydrazone analogues. In this study, the Glide algorithm [137] was utilized, which is considered to be one of the most efficient and accurate virtual screening tools [138] for structure-based virtual screening of the guanylhydrazone analogues inside the AdoMetDC binding site. All docking calculations were performed by using VdW scaling of 0.8 for ligand atoms, a maximum of 3 poses per ligand and extra-precision (XP), a rather extensive, accurate and time- and CPU- demanding mode [139].

2.7 QSAR analysis

Introduction

Although QSAR was first developed more than 55 years ago [140], it still remains one of the most promising research areas in medicinal chemistry and cheminformatics. QSAR aims to reveal a quantitative correlation between the structural features of chemical entries and their many different properties, such as continuous (pIC_{50}, pEC_{50}, Ki, *etc.*), categorical/binary (active, inactive, toxic, nontoxic, *etc.*) and biological/toxicological. To this end, the main strategy involves the generation of a statistical linear or non-linear regression model that matches experimental values to a diverse set of molecular descriptors determined from the structure of the compounds [141]. ~~Chemical descriptors constitute the basis of QSAR modeling and reflect a plethora of chemical structure representation. These molecular descriptors have been categorized into different classes, including constitutional, geometrical, topological, quantum chemical and so on, with 2D (two-dimensional) being the most popular among drug developers.~~ Molecular descriptors compose the basis of QSAR modeling and represent different levels of chemical structure representation ranging from single physico-chemical properties (1D QSAR) to three-dimensional structures (3D QSAR), and even more intricate, multidimensional approaches like simulation of induced fit and solvation scenarios (5D and 6D QSAR) [142]. The success of QSAR analysis depends on the quality of the input data, selection of appropriate descriptors and statistical methods to validate the developed model. QSAR analysis has yielded quite a few success stories, ~~regarding~~ including currently approved drugs [143-145]. In the framework of this study, the Canvas cheminformatics software package was utilized [146], in an attempt to connect ones and zeros with reliable SAR predictions. Canvas provides a wide range of applications for structural and data analysis, including 2D and 3D fingerprints, similarity searching, as well as building regression and classification models.

Protocol

Preparation of the guanylhydrazone analogues was performed with Ligprep, as previously described [135], with the exception of generating only the most probable ionization and tautomeric state of each analogue, chosen on the basis of energetic considerations. Then, prepared compounds were introduced into the Canvas interface and the complete set of 498 physicochemical, topological, Ligfilter and Qikprop descriptors were determined for all entries. A total of nine fingerprints were calculated using default atom typing and scaling parameters. Seven 2D fingerprints, (linear, radial, dendritic, MOLPRINT 2D, atom pairs, atom triplets, and topological torsions) and two 3D pharmacophore fingerprints (2p and 3p pharmacophore), with Tanimoto similarity were used for ranking. A detailed description of each fingerprint has been ~~realized~~ established by Sastry and colleagues [147]. Statistical regression models were then generated, utilizing three diverse and well-established statistical methods, namely Multiple Linear Regression (MLR), Partial Least Squares

regression (PLS) and Kernel-based Partial Least Squares regression (KPLS), in order to successfully and efficiently correlate the cell-based *in vitro* activity of the guanylhydrazone analogues ~~on~~ against *T. brucei* to the aforementioned molecular descriptor and 2D/3D fingerprints. The initial approach included the implementation of all guanylhydrazone analogues in the training set. As expected, the compounds with none or marginal activity against *T. brucei* (**G12**, **G14**, **G15** and **G20**) seemed to impede the generation of an accurate and reliable model. Indicatively, standard deviation (SD), as well as the coefficient of determination (R^2), resulted from MLR analysis, and proved that the model containing all analogues was quite questionable (SD = 1.526; R^2 = 0.5720). Therefore, in order to improve the predictivity of the model, only active compounds were utilized. A training set of 27 active compounds were analysed through MLR, PLS and KPLS regression functions with a 20% of random test set assignment for model evaluation. ~~The option of five best subsets was used for MLR, attempting to find the highest-ranking model containing said number of independent variables, utilizing a simulated annealing Monte Carlo technique.~~ For each MLR model generated, the option of "best subsets" was chosen, attempting to find the highest-ranking models containing five independent variables. Default settings were used for the simulated annealing Monte Carlo technique. Selection of the best MLR model was performed through careful evaluation of each model, ~~considering~~ taking into account intercorrelation between selected independent variables. For both PLS and KPLS, four factors were used. Hierarchical clustering of the guanylhydrazone analogues was attempted, based on the 2D fingerprint of atom pairs. Analogues were divided into three clusters, which were then statistically processed as previously described. Note that this approach did not yield any meaningful results.

3. Results and Discussion

3.1 Chemistry

**Synthesis of Series 1 compounds**

For the synthesis of the starting ketones **3** and **4** (Scheme **1**), adamantan-2-one **1** was first converted to 4-oxahomoadamantan-5-one **2** *via* a selenium dioxide mediated oxidation. Lactone **2** was heated

with a 50% sulfuric acid and yielded a mixture consisting of the axial and the equatorial isomer of **3**, in an approximate ratio of 5 : 1. Oxidation of the latter with chromic acid afforded the adamantane dione **4** [148].
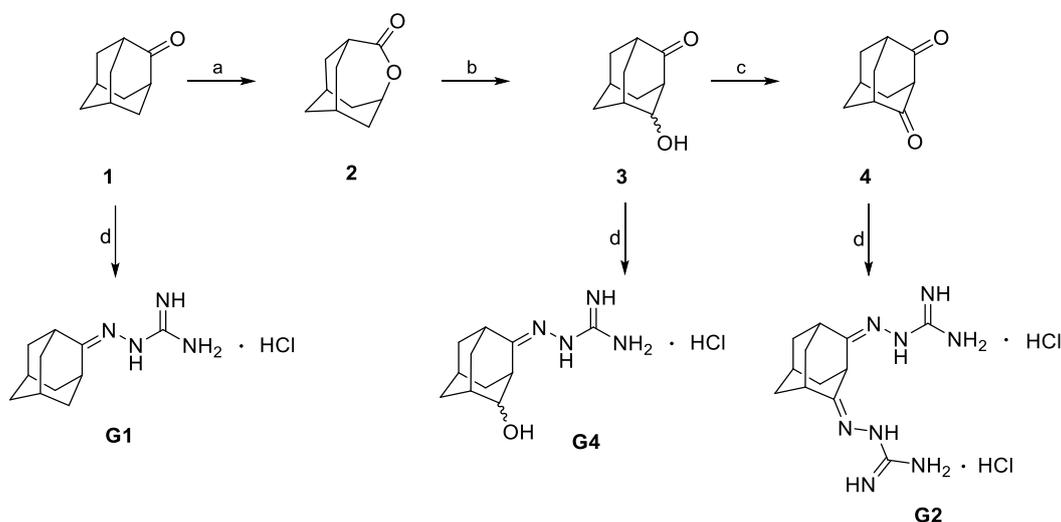
Scheme 1. Synthetic route to the starting compounds **3** and **4** and synthesis of mono and bis(guanylhydrazone) adamantanes **G1, G2** and **G4**. Reagents and conditions: (a) SeO_2, H_2O_2, t-BuOH, 96%; (b) H_2SO_4 (50%), 5 h, 90 °C; (c) H_2CrO_4; (d) $H_2NNHC(=NH)NH_2 \cdot HCl$, EtOH, reflux, 5 h, 99% (**G1**), 97% (**G2**) and 94% (**G4**) [114,148].

The synthetic route for the formation of starting compounds **9** and **10** is described in Scheme **2**. Oxygen-containing adamantane analogues are provided by functionalization of the adamantane core with the use of oxidizing agents. Initially the adamantane hydroxylation was performed upon treatment with fuming sulfuric acid ($H_2O_7S_2$). The products of the oxidative procedure are three diols obtained in different ratio. In fuming acid with a SO_3 percentage of 20%, 1,4-adamantane diol **6** is the main product in an overall yield of 45 – 50%. 1,3-Diol **7** and 2,6-diol **8** were also formed with 15 – 20% and 5 – 10% yields, respectively. The mixture of diols **6**, **7** and **8** was subjected to oxidation with chromic acid to give 5-hydroxyadamantan-2-one/1-hydroxyadamantan-4-one **9** and adamantane-2,6-dione **10** [149].
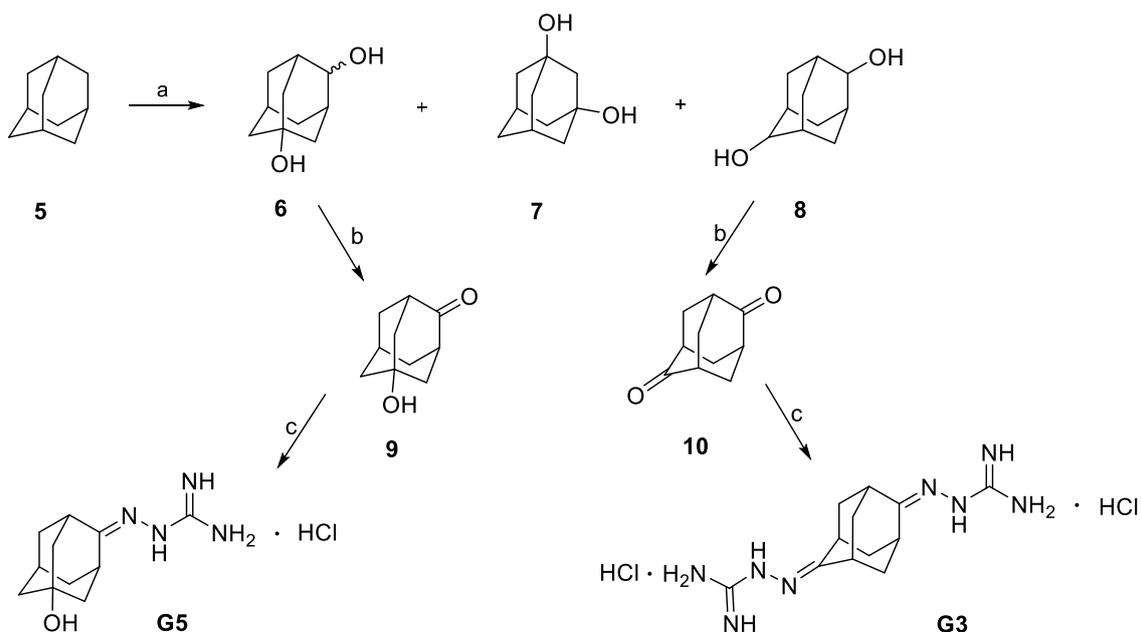
Scheme 2. Synthetic route to the starting compounds **9** and **10** and synthesis of mono and bis(guanylhydrazone) adamantanes **G3** and **G5**, respectively. Reagents and conditions: (a) 20% SO_3 (10 °C), 20 min, 25 °C then 100 °C, 2 h; (b) CrO_3, H_2O, 30 min, 70 °C; (c) $H_2NNHC(=NH)NH_2 \cdot$ HCl, EtOH, reflux, 5 h, 98% (**G3**) and 99% (**G5**) [114,149].

Adamantyl guanylhydrazones **G1** – **G5** used in this study were synthesized according to the previously published procedure by condensing the corresponding adamantanone with aminoguanidine hydrochloride (Schemes **1** and **2**) almost quantitatively. Note that compounds **G2** and **G4** (Scheme **1**) have been isolated as a mixture of diastereoisomers and derivative **G2** has three possible diastereoisomers while derivative **G4** has four possible diastereoisomers. However, for guanylhydrazones **G1** (Scheme **1**), **G3** and **G5** (Scheme **2**), only one diastereomeric form is possible due to molecular symmetry [114].

Synthesis of Series 2 compounds

The synthesis of 1,2-disubstituted adamantane derivatives was the key step for the preparation of analogues described in this study and was achieved by rearrangement of the protoadamantane framework [150]. The starting compound, protoadamantanone **13**, was synthesized by Majerski's group for the first time in 1979. As shown in Scheme **3**, the commercially available adamantan-1-ol **11** reacted with lead tetraacetate and iodine in benzene as a solvent, and the iodo ketone **12** that was generated was refluxed with potassium hydroxide to provide protoadamantanone **13** in yields ranging from 71% to 82% [151]. The amount of the unreacted starting alcohol was decreased by heating the

mixture composed of adamantan-1-ol **11**, lead tetraacetate and iodine for 2 h at 75 – 76 °C. The target compound **13** was then produced, almost pure, in excellent yields [152].
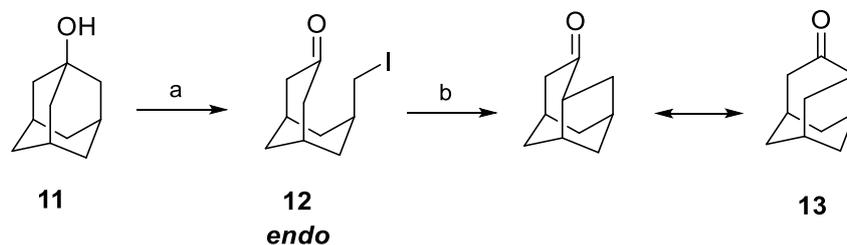
Scheme 3. Synthesis of protoadamantanone. Reagents and conditions: (a) Pb(OAc)$_4$, I$_2$, C$_6$H$_6$, 70 – 75 °C (b) KOH, MeOH, reflux [151].

As depicted in Scheme **4**, synthesis of the starting ketones **18a – d** [112] proceeded with formation of the acetylenic alcohols **14a – d**. More specifically, protoadamantanone **13** reacted with the appropriate lithiated acetylide, which was prepared *in situ* by addition of a substituted acetylene to a solution of butyllithium, to give the desired compounds **14a – d** as a mixture of *endo/exo* isomers (1 : 1) in an overall yield of 82 – 95%. Catalytic hydrogenolysis of the latter with Adams' catalyst yielded the corresponding saturated isomeric alcohols **15a – d**. The mixture was refluxed with formic acid and the formate esters immediately underwent an intramolecular metathesis to give analogues **16a – d**. Subsequent saponification of the intermediates **16a – d** in the presence of an aqueous sodium hydroxide solution led to alcohols **17a – d** in excellent yields which underwent Jones oxidation to form the target 1-alkyl-adamantan-2-ones **18a – d** almost quantitatively [112].

For the synthesis of 1-alkyl-adamantane 2-guanylhydrazones **G6 – G9**, the starting ketones **18a – d** were refluxed with aminoguanidine bicarbonate in the presence of concentrated hydrochloric acid (pH ~ 2) and ethanol as a solvent. The target compounds **G6 – G9** were obtained in an overall yield of 85 to 94% [112].
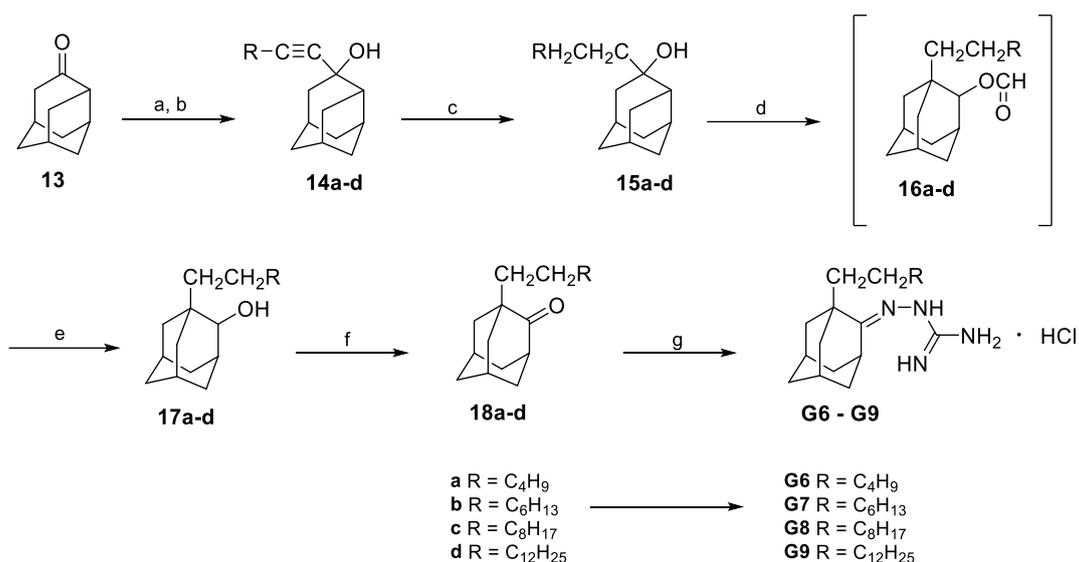
Scheme 4. Synthetic route to the starting compounds 1-alkyl-adamantan-2-ones **18a** – **d** and synthesis of 1-alkyl-adamantane 2-guanylhydrazones **G6** – **G9**. Reagents and conditions: (a) R–C≡CH, *n*-BuLi, dry THF, 1 h, 0 °C then 20 h, rt, 82 – 95%; (b) H_2O; (c) H_2/PtO_2, EtOH, 4 h, rt, 55 psi; (d) HCOOH, reflux, 30 min; (e) NaOH, EtOH/H_2O, reflux, 2 h, 91 – 96%; (f) CrO_3, aq. H_2SO_4 (8N), acetone, 15 °C then rt, 1h, 95 – 98%; (g) $H_2NNHC(=NH)NH_2 \cdot HCO_3$, conc. HCl (pH ~ 2), EtOH, reflux, 5 h, 85 – 94% [112].

Thiosemicarbazones **G10** and **G11** (Scheme **5**), possessing a *n*-hexyl and a *n*-tetradecyl chain, respectively, were obtained by condensation of thiosemicarbazide with the structurally related ketones **18a** and **18d** [112].
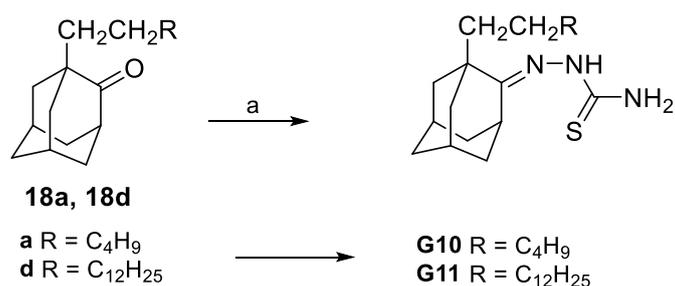

Scheme 5. Synthesis of the 1-alkyl-adamantane 2-thiosemicarbazones **G10** and **G11**. Reagents and conditions: (a) $H_2NNHC(=S)NH_2$, EtOH, reflux, 5 h, 82% (**G10**) and 89% (**G11**) [112].

Synthesis of Series 3 compounds

Synthesis of the adamantane diol **25** (Scheme **6**) [152] starts with a Reformatsky reaction between protoadamantanone **13** and bromoacetic acid ethyl ester in the presence of zinc metal, as shown in

Scheme **6**. Upon saponification with sodium hydroxide in an EtOH/H$_2$O solution, the hydroxyacid **19** was obtained in poor yields along with some starting ketone. Alternatively, when protoadamantanone **13** was used as starting material and treated with LiCH$_2$COOCH$_3$, followed by hydrolysis of the intermediate ester **20** under basic conditions, the desired compound **19** was afforded with an improved yield of 98%. LiCH$_2$COOCH$_3$ was prepared by lithium bis(trimethylsilyl)amide and methyl ethanoate in one pot. Then, the hydroxyacid **19** provided a mixture of the respective ester **21** as a major product and the lactone **22** in traces, under reflux with formic acid. Subsequent saponification of the mixture and oxidation of the intermediate **23** with a solution of chromium trioxide in diluted sulfuric acid generated the ketoacid **24**. Finally, lithium aluminum hydride catalyzed reduction of the latter gave rise to the desired diol **25** [152].

1-Alkyloxyadamantane 2-guanylhydrazones **G12** – **G15** and 1-benzyloxyadamantane 2-guanylhydrazone **G20** were prepared as outlined in Scheme **6**. The intermediate 1-alkoxy alcohols **26a** – **d** were synthesized *via* alkylation with the appropriate alkyl bromide in the presence of sodium hydride in *N,N*-dimethylformamide. Under similar reaction conditions, benzyl chloride was used as an alkylating agent for the formation of the benzyl substituted alkoxy alcohol **26e**. The aforementioned intermediates were oxidized to the respective ketones **27a** – **e** by chromium trioxide in an aqueous sulfuric acid solution. Treatment of the latter with aminoguanidine bicarbonate, upon pH adjustment to 2 with hydrochloric acid, yielded the guanylhydrazones **G12** – **G15** and **G20** [113].
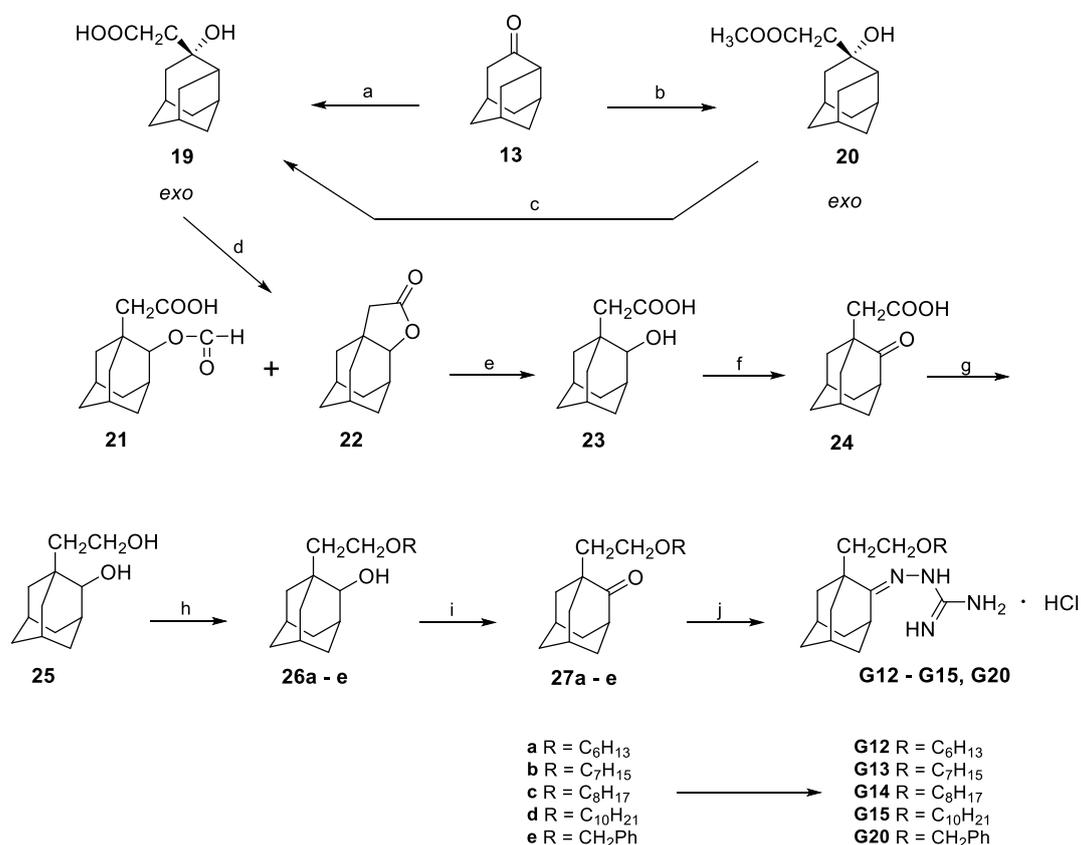
Scheme 6. Synthesis of the starting adamantane diol **25** and synthetic procedure for the preparation of the 1-alkyloxy and 1-benzyloxyadamantane 2-guanylhydrazones **G12** – **G15** and **G20**, respectively. Reagents and conditions: (a) i) BrCH$_2$COOEt, Zn, C$_6$H$_6$, reflux; ii) NaOH, EtOH/H$_2$O, 90 °C, 2.5 h, (HCl), 25%; (b) [(CH$_3$)$_3$Si]$_2$NLi, CH$_3$COOCH$_3$, dry THF, –75 °C, 20 min and –60 °C, 30 min; (c) NaOH, EtOH/H$_2$O, 90 °C, 2.5 h, (HCl), 98%; (d) HCOOH, reflux, 30 min; (e) NaOH, EtOH/H$_2$O, 90 °C, 2.5 h, (HCl), 87%; (f) CrO$_3$, aq. H$_2$SO$_4$ (1M), acetone, 15 °C then rt, 24h, 92%; (g) LiAlH$_4$, dry Et$_2$O, reflux; (h) For compounds **26a** – **d**: i) NaH, dry DMF, 20 min, rt; ii) RBr, dry DMF, 16 h, 105 °C, 69 – 87%; For compound **26e**: i) NaH, dry DMF, 20 min, rt; ii) PhCH$_2$Cl, dry DMF, 2 h, rt; iii) 1 h, 60 °C; iv) 16 h, rt, 82%; (i) CrO$_3$, aq. H$_2$SO$_4$ (8N), acetone, 15 °C then rt, 1h, quantitative yield; (j) H$_2$NNHC(=NH)NH$_2$ · HCO$_3$, conc. HCl (pH ~ 2), EtOH, reflux, 6 h, 56 – 89% [113,152].

For the synthesis of the (butoxyethoxy)ethyl substituted adamantane 2-guanylhydrazone **G17** (Scheme **7**) [113], the adamantane diol **25** was first treated with sodium hydride and the resulting alkoxide anion was subsequently reacted with ethyl bromoacetate. The intermediate ethanoate was saponified, and upon acidification with concentrated hydrochloric acid, the hydroxy acid **28** was produced with an overall yield of 85%. The latter was reduced with lithium aluminum hydride to the respective diol **29,** which was alkylated with 1-bromobutane in the presence of sodium hydride in poor yields. Jones oxidation of the alcohol **30**, followed by coupling of the precursor ketone **31** with aminoguanidine bicarbonate, as previously described, led to the desired compound **G17** [113].
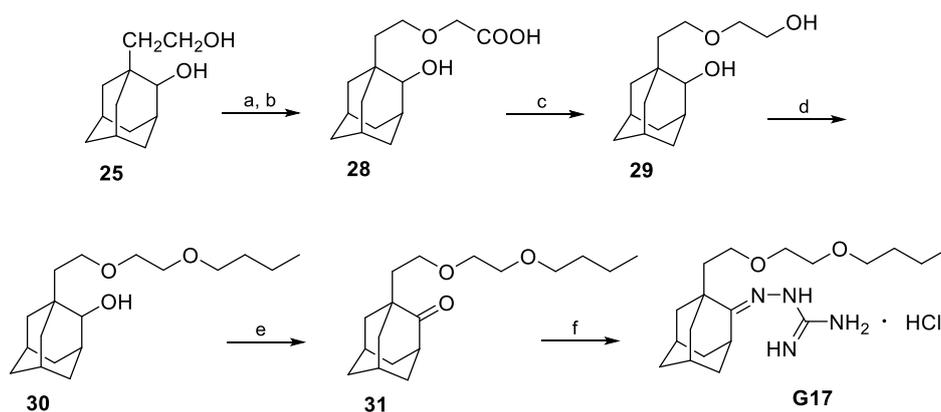
Scheme 7. Synthetic procedure for the preparation of 1-(butoxyethoxy)ethyladamantano 2-guanylhydrazone **G17**. Reagents and conditions: (a) i) NaH, dry DMF, 20 min, rt; ii) BrCH$_2$COOCH$_2$CH$_3$, dry DMF, 8 h, 110 °C; (b) NaOH, EtOH/H$_2$O, 2 h, 100 °C, conc. HCl, 85%; (c) LiAlH$_4$, dry THF, reflux, 8 h, 96%; (d) i) NaH, dry DMF, 20 min, rt; ii) CH$_3$CH$_2$CH$_2$CH$_2$Br, dry

DMF, 15 h, 105 – 110 °C, 18%; (e) CrO$_3$, aq. H$_2$SO$_4$ (8N), acetone, 15 °C then rt, 30 min, 89%; (f) H$_2$NNHC(=NH)NH$_2$ · HCO$_3$, conc. HCl (pH ~ 2), EtOH, reflux, 6 h, 79% [113].

As depicted in Scheme **8** [113], a five-step synthetic route was applied for the preparation of the guanylhydrazone **G18**. Starting from diol **25**, the ethyl ester **32** was obtained by alkylation with ethyl 5-bromovalerate. Then, conversion of **32** to diol **33** was carried out by reduction mediated by lithium aluminum hydride. Subsequent alkylation of **33**, to the corresponding methoxy congener **34** was achieved with methyl iodide and sodium hydride as a base. Employment of the above-mentioned procedure, oxidation of **34** with Jones reagent and condensation of the intermediate ketone **35** with aminoguanidine bicarbonate afforded the analogue **G18** in 69% yield [113].
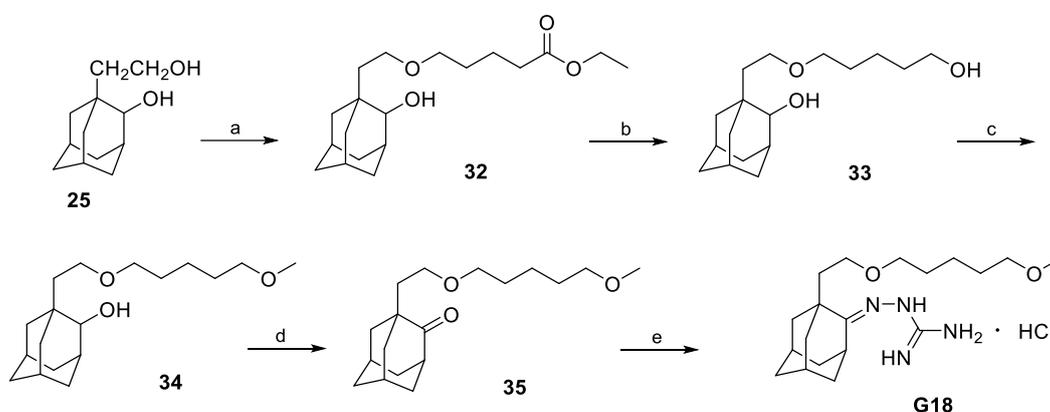
Scheme 8. Synthetic procedure for the preparation of 1-(methoxypentyloxy)ethyladamantano 2-guanylhydrazone **G18**. Reagents and conditions: (a) i) NaH, dry DMF, 30 min, rt; ii) Br(CH$_2$)$_4$COOCH$_2$CH$_3$, dry DMF, 15 h, 105 °C, 32%; (b) LiAlH$_4$, dry Et$_2$O, reflux, 15 h, 88%; (c) i) NaH, dry DMF, 20 min, rt; ii) CH$_3$I, dry DMF, 24 h, rt, 40%; (d) CrO$_3$, aq. H$_2$SO$_4$ (8N), acetone, 15 °C then rt, 30 min, 89%; (e) H$_2$NNHC(=NH)NH$_2$ · HCO$_3$, conc. HCl (pH ~ 2), EtOH, reflux, 5 h, 69% [113].

The synthetic route to 1-benzyloxyadamantane 2-guanylhydrazone **G19** [113] is depicted in Scheme **9**. For the preparation of the adamantane diol **37** [100], protoadamantanone **13** was treated with dimethylsulfonium methylide to give a mixture of *endo/exo* epimers of the epoxide **36** in a 1:15 ratio. Then, oxirane ring opening under acidic conditions in acetone produced the target compound **37**. Alternatively, the cleavage of oxirane rings is pronounced in the presence of formic acid. Reaction of epoxide **36** with formic acid, upon heating, yielded the respective formate diester, which was further saponified to provide diol **37** [100].

The intermediate 1-alkoxy alcohol **38** was synthesized *via* alkylation of **37** with benzyl chloride, using sodium hydride as a base and *N,N*-dimethylformamide as solvent. Alcohol **38** was oxidized to the corresponding ketone **39** by chromium trioxide in an aqueous sulfuric acid solution. The guanylhydrazone **G19** was prepared by reacting the precursor ketone **39** with aminoguanidine bicarbonate in the presence of hydrochloric acid with an overall yield of 65% [113].
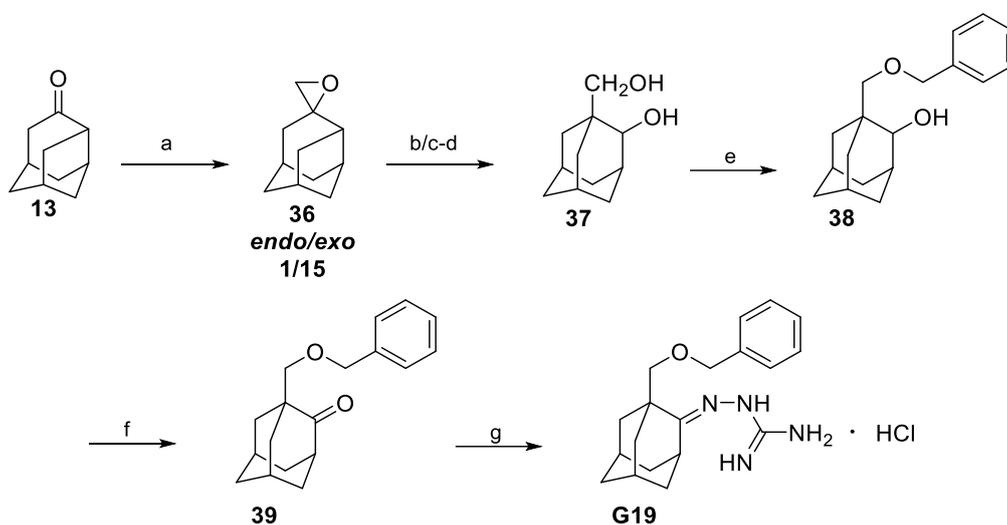
Scheme 9. Synthesis of the starting adamantane diol **37** and synthetic procedure for the preparation of 1-benzyloxyadamantane 2-guanylhydrazone **G19**. Reagents and conditions: (a) $(CH_3)_2S=CH_2$, DMSO, 3 h, 25 °C and 8 h, 55 °C; (b) H_2SO_4/H_2O (0.085 M), acetone, T °C or (c) HCOOH, 30 min, T °C; (d) NaOH, EtOH/H_2O, T °C; (e) i) NaH, dry DMF, 20 min, rt; ii) $PhCH_2Cl$, dry DMF, 2 h, rt; iii) 1 h, 60 °C; iv) 16 h, rt, 80%; (f) CrO_3, aq. H_2SO_4 (8N), acetone, 15 °C then rt, 1h, quantitative yield; (g) $H_2NNHC(=NH)NH_2 \cdot HCO_3$, conc. HCl (pH ~ 2), EtOH, reflux, 6 h, 65% [100,113].

The key intermediate **43** [152] was obtained by a four-step synthetic procedure as depicted in Scheme **10**. Protoadamantanone **13** undergoes a typical Grignard reaction with the dimagnesium derivative of propargylic alcohol to form the acetylenic diol **40**, which was hydrogenated in the presence of platinum (IV) oxide as a catalyst, to the respective saturated diol **41**. The diol **43** was produced in good yields upon heating of diol **41** with formic acid and subsequent saponification of the intermediate diester **42** [152].

Compound **43** was alkylated with 1-bromohexane and benzyl chloride to give the alcohols **44a** and **44b**, respectively. Employment of the previously described experimental protocol for the preparation of guanylhydrazones **G12** – **G15** and **G20** (Scheme **6**), Jones oxidation of the intermediates **44a** and **44b,** and subsequent condensation of ketones **45a** and **45b** with aminoguanidine bicarbonate, led to the desired analogues **G16** and **G21** in 94% and 53% yields, respectively [113].
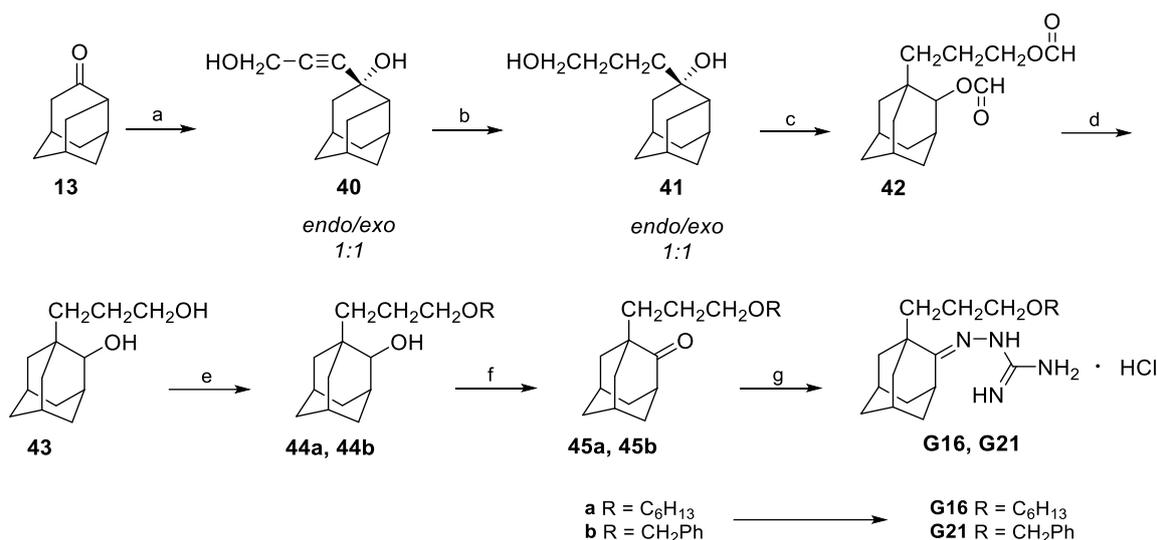
Scheme 10. Synthesis of the starting adamantane diol **43** and synthetic procedure for the preparation of 1-alkyloxy and 1-benzyloxy propyladamantane 2-guanylhydrazones **G16** and **G21**. Reagents and conditions: (a) BrMg–C≡C–CH$_2$OMgBr, dry THF, reflux, 6 h and 24 h, 20 °C; ii) NH$_4$Cl, H$_2$O, 82%; (b) H$_2$/PtO$_2$, 97%; (c) HCOOH, reflux, 30 min, 100%; (d) NaOH, EtOH/H$_2$O, reflux, 2 h, 81%; (e) for compound **44a**: i) NaH, dry DMF, 20 min, rt; ii) C$_6$H$_{13}$Br, dry DMF, 16 h, 105 °C, 78%; for compound **44b**: i) NaH, dry DMF, 20 min, rt; ii) PhCH$_2$Cl, dry DMF, 2 h, rt; iii) 1 h, 60 °C; iv) 16 h, rt, 85%; (f) CrO$_3$, aq. H$_2$SO$_4$ (8N), acetone, 15 °C then rt, 1h, quantitative yield; (g) H$_2$NNHC(=NH)NH$_2$ · HCO$_3$, conc. HCl (pH ~ 2), EtOH, reflux, 6 h, 94% (**G16**) and 53% (**G21**) [113,152].

Synthesis of Series 4 compounds

The preparation of 1-phenyl substituted adamantan-2-one **49a** [153] was achieved following a synthetic procedure similar to that of 1-alkyl-adamantan-2-ones **18a** – **d** (Scheme **4**). Starting from protoadamantanone **13**, the tertiary alcohol **46a** was obtained upon treatment with phenyl lithium to facilitate the formation of the C–C bond. Employment of the previously described methodology, heating with formic acid to produce the formate **47a**, saponification of the latter and oxidation with Jones reagent of the intermediate alcohol **48a,** gave the desired ketone **49a** in good yields [153]. The starting compound 1-benzyladamantan-2-one **49b** was synthesized as described above; with the only exception being that benzylmagnesium bromide reacted with protoadamantanone **13** instead of phenyl lithium. Following the similar procedure for the formation of guanylhydrazones **G6** – **G9** (Scheme **4**), 1-phenyl adamantane 2-guanylhydrazone **G22** and 1-benzyladamantane 2-guanylhydrazone **G23** were obtained almost quantitatively and in 96% and 78% yields, respectively [112].

Scheme 11. Synthetic route to the starting compounds 1-phenyl and 1-benzyl adamantan-2-ones **49a** and **49b,** respectively and synthetic route for the preparation of 1-phenyl and 1-benzyladamantane 2-guanylhydrazones **G22** and **G23**, respectively. Reagents and conditions: (a) C_6H_5Li in $[CH_3(CH_2)_3]_2O$ (2M), $PhCH_2MgBr$, dry THF, 1 h, 20 °C, 96%; (b) H_2O; (c) HCOOH, reflux, 30 min; (d) NaOH, $EtOH/H_2O$, T °C, 2 h, 96%; (e) CrO_3, aq. H_2SO_4 (8N), acetone, 15 °C then rt, 1h; (f) $H_2NNHC(=NH)NH_2 \cdot HCO_3$, conc. HCl (pH ~ 2), EtOH, reflux, 5 h, 96% (**G22**) and 78% (**G23**) [112,153].

The synthesis of 1-(benzyloxy)adamantane 2-guanylhydrazones **G24** and **G25** [113] was initiated with conversion of protoadamantanone **13** to the tertiary alcohols **50a** and **50b,** upon treatment with the appropriate organomagnesium bromide *via* a Grignard reaction. According to the procedure described in Scheme **12**, the intermediates **50a** and **50b** were esterified with formic acid, and upon self-metathesis, the respective formates (not presented in **Scheme 12**) were obtained. Saponification of the latter afforded the corresponding alcohols which underwent Jones oxidation. The resulting ketones **51a** and **51b** were coupled with aminoguanidine bicarbonate in an ethanolic solution under acidic conditions. The desired guanylhydrazones **G24** and **G25** were isolated as hydrochloride salts in overall yields of 79% and 66%, respectively [113].

Scheme 12. Synthetic procedure for the preparation of 1-(benzyloxy)adamantane 2-guanylhydrazones **G24** and **G25**. Reagents and conditions: (a) XC_6H_4MgBr, dry THF; (b) HCOOH, reflux, 30 min; (c) NaOH, EtOH/H_2O, 2 h, T °C; (d) CrO_3, aq. H_2SO_4 (8N), acetone, 15 °C then rt, 30 min, 93% (**51a**) and 91% (**51b**); (e) $H_2NNHC(=NH)NH_2 \cdot HCO_3$, conc. HCl (pH ~ 2), EtOH, reflux, 5 h, 79% (**G24**) and 66% (**G25**) [113].

Synthesis of Series 5 compounds

For the preparation of starting ketone **53**, adamantanecarbonyl chloride **52** was allowed to react with phenylmagnesium bromide in anhydrous THF and the target compound **53** was obtained in 67% yield [154]. The novel guanylhydrazone **G26** was prepared following the synthetic protocol described above for the formation of analogues **G6** – **G9** (Scheme **4**) [112].
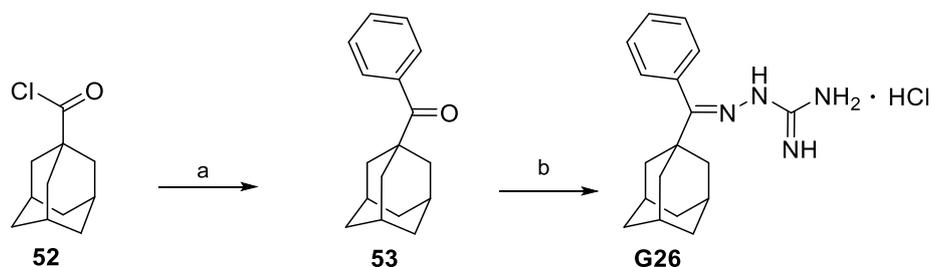
Scheme 13. Synthesis of 1-adamantyl methyl guanylhydrazone **G26**. Reagents and conditions: (a) PhMgBr, dry THF (–78 °C), 2 h, rt, Ar, 67%; (b) $H_2NNHC(=NH)NH_2 \cdot HCO_3$, conc. HCl (pH ~ 2), EtOH, reflux, 5 h, almost quantitatively [112,154].

The synthetic route to 2-adamantyl phenyl ketone **57** (Scheme **14**) involved a typical Horner-Wadsworth-Emmons reaction of 2-adamantanone **1** with (methoxymethyl)triphenylphosphonium chloride, in the presence of *n*-BuLi as a base, to deprotonate the latter under anhydrous conditions to give the unsaturated ether **54**. Acid-promoted hydrolysis of the enol ether **54** with a 70% perchloric

acid generated the aldehyde **55** in good yields. Then, the latter reacted with phenylmagnesium bromide to give the respective alcohol **56**. A pyridinium chlorochromate (PCC) catalyzed oxidation of **56** yielded ketone **57,** almost quantitatively [155]. The reaction of equimolar quantities of the precursor **57** with aminoguanidine bicarbonate under the same conditions previously mentioned, produced the novel guanylhydrazone **G27** almost quantitatively [112].
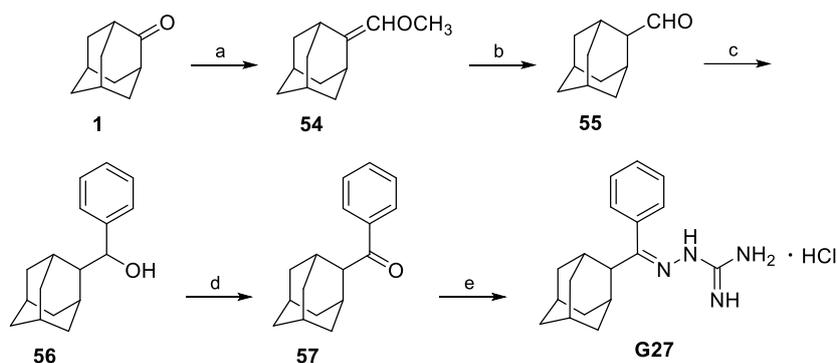

Scheme 14. Synthesis of 2-adamantyl methyl guanylhydrazone **G27**. Reagents and conditions: (a) $CH_3OCH_2P(C_6H_5)_3Cl$, *n*-BuLi, dry Et_2O (0 °C), 1 h then 15 h, rt, N_2; (b) $HClO_4$ 70%/H_2O, 78%; (c) i) PhMgBr, dry THF (0 °C), 5 h, rt; ii) NH_4Cl, H_2O, 89%; (d) $[C_5H_5NH]^+[CrO_3Cl]^-$, CH_3COONa, CH_2Cl_2, 2 h, 95%; (e) $H_2NNHC(=NH)NH_2 \cdot HCO_3$, conc. HCl (pH ~ 2), EtOH, reflux, 5 h, almost quantitatively [112,155].

The formation of guanylhydrazone **G28** is presented in Scheme **15**. The synthesis of the intermediate epoxide **58** was achieved *via* the Corey-Chaykovsky reaction which involves the base-mediated addition of trimethylsulfoxonium iodide to 1-phenyl adamantan-2-one **49a**. Sodium hydride was used as a base and the reaction was performed in anhydrous dimethyl sulfoxide. Afterwards, the oxirane ring was cleaved by boron trifluoride diethyl etherate and subsequent rearrangement provided the aldehyde **59**. Upon Jones oxidation, carboxylic acid **60** was produced, and it reacted with thionyl chloride to give the respective chloride. Finally, treatment with aluminum chloride in carbon disulphide drives cyclization of the latter to ketone **61,** almost quantitatively [156]. Following the general procedure presented in Scheme **4**, the novel guanylhydrazone **G28** was obtained upon treatment with aminoguanidine bicarbonate under acidic conditions, with an overall yield of 83% [112].
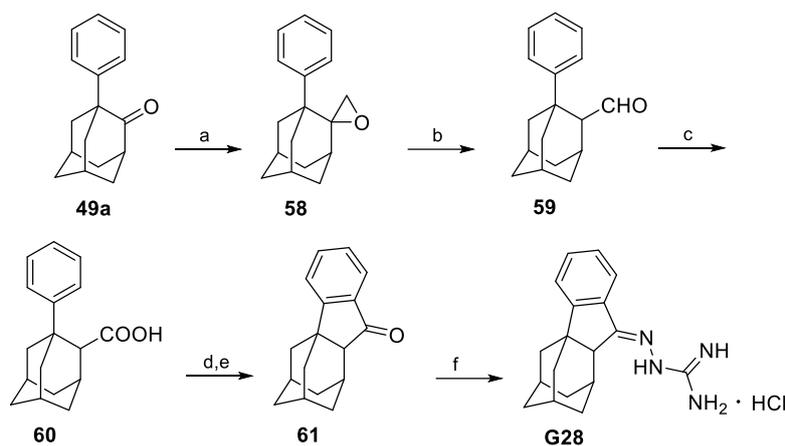
Scheme 15. Synthesis of guanylhydrazone **G28**. Reagents and conditions: (a) (CH$_3$)$_3$SO$^+$I$^-$, NaH, dry DMSO, 30 min, 20 °C then 2 h, 55 – 58 °C; (b) BF$_3$ · Et$_2$O, dry C$_6$H$_6$; (c) CrO$_3$, aq. H$_2$SO$_4$ (8N), acetone, 15 °C then rt, overnight; (d) SOCl$_2$, 15 min, 65 °C; (e) AlCl$_3$, CS$_2$, 30 min, rt then reflux, 30 min, quantitatively; (f) H$_2$NNHC(=NH)NH$_2$ · HCO$_3$, conc. HCl (pH ~ 2), EtOH, reflux, 5 h, 83% [112,156].

As previously described [112], the newly synthesized guanylhydrazones **G29** – **G31** were prepared by condensation of the commercially available precursors **62a** – **c** with a suspension of aminoguanidine hydrochloride. The latter was prepared in turn from a suspension of aminoguanidine bicarbonate and an excess of concentrated hydrochloric acid upon pH adjustment to 2. The desired compounds were produced almost quantitatively, with the only exception being **G30,** which was isolated in an overall yield of 28%.

62a - c

a R$_1$ = fluorene
b R$_1$ = dibenzosuberane
c R$_1$ = 4-phenyl cyclohexane

G29 - G31

G29 R$_1$ = fluorene
G30 R$_1$ = dibenzosuberane
G31 R$_1$ = 4-phenyl cyclohexane
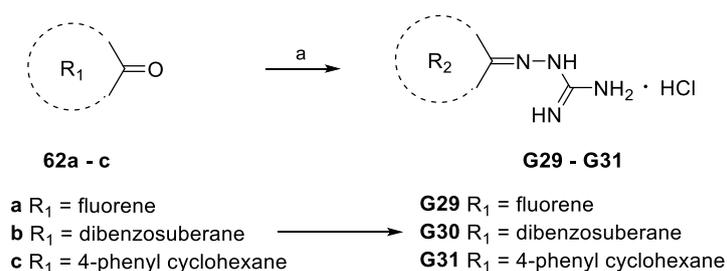
Scheme 16. Synthesis of novel guanylhydrazones **G29** – **G31**. Reagents and conditions: (a) H$_2$NNHC(=NH)NH$_2$ · HCO$_3$, conc. HCl (pH ~ 2), EtOH, reflux, 5 h, 28 – 98%.

3.2 Biological evaluation

Series 1-5 analogues (**G1** – **G31**) were assessed based on their ability to inhibit proliferation of cultured bloodstream form *T. brucei in vitro*. Series 5 analogues (**G26** – **G31**) were also tested against *T. cruzi* epimastigotes *in vitro*. The EC_{50} and EC_{90} values for each compound are presented in Tables **1** – **5**. As shown, 20 (**G3**, **G8** – **G11**, **G13**, **G16** – **G19**, **G21**, **G22** – **G25**, **G26** – **G29** and **G31**) out of the 31 tested compounds had promising EC_{50} values in the low micromolar to sub micromolar range against *T. brucei*. Most of the compounds were evaluated as hydrochloride salts, with the only exception being analogues **G10** and **G11**, which were tested as free bases.

Cmpd	Structure	*T. brucei* EC_{50} (μM) [a]	*T. brucei* EC_{90} (μM) [a]
Table 1 Activity of the adamantane mono(guanylhydrazone) analogues **G1**, **G4** and **G5** and the bis(guanylhydrazone) analogues **G2** and **G3** against cultured bloodstream form *T. brucei* (pH 7.4) *in vitro*.			
G1		56.9 ± 3.3	88.6 ± 13.1
G2		167 ± 6	214 ± 4
G3		9.67 ± 1.21	21.7 ± 3.9
G4		>300	>300
G5		>300	>300

[a] *Concentrations required to inhibit growth of T. brucei by 50% and 90%, respectively. EC_{50} and EC_{90} data are the mean of triplicate experiments ± SEM.*

As shown in Table **1**, the 2-(guanylhydrazone)adamantane **G1** exhibited moderate inhibitory activity in the micromolar range, with an EC_{50} value of 56.9 μM. Introduction of a second guanylhydrazone group at position 4 of the adamantane ring resulted in a 3-fold decrease in the activity of **G2** (EC_{50} = 167 μM). It is of great interest that shifting the pharmacophore moiety from position 4 to position 6 of the adamantane cage increased the activity to the low micromolar range. The bis(guanylhydrazone) analogue **G3** was 17 times more potent (EC_{50} **G3** = 9.67 μM) than the structurally related compound

G2. Incorporation of the OH functional group at position 4 of mono(guanylhydrazone) analogue **G1** led to a substantial loss of activity for the **G4** (EC$_{50}$ = >300 μM). Changing the position of the hydroxyl group to the vicinal carbon atom yielded compound **G5**, which also showed no activity at the highest concentration tested (~300 μM).

Cmpd	Structure	*T. brucei* EC$_{50}$ (μM) [a]	*T. brucei* EC$_{90}$ (μM) [a]
	Table 2 Activity of the 1-alkyl-2-guanylhydrazone adamantanes **G6** – **G9** and the 1-alkyl-2-thiosemicarbazone adamantanes **G10** and **G11** against cultured bloodstream form *T. brucei* (pH 7.4) *in vitro*.		
G6		>6.0	-
G7		>6.0	-
G8		0.09 ± 0.02	0.11 ± 0.00
G9		0.84 ± 0.50	1.30 ± 0.50
G10		2.81 ± 0.09	5.64 ± 0.54
G11		0.42 ± 0.04	0.54 ± 0.02

[a] *Concentrations required to inhibit growth of T. brucei by 50% and 90%, respectively. EC$_{50}$ and EC$_{90}$ data are the mean of triplicate experiments ± SEM.*

Compounds that constitute Series 2, characterized by a lipophilic tail in position 1 of the adamantane core, were more potent than those of Series 1. In particular, the EC$_{50}$ values were at low micromolar to submicromolar levels (2.81 μM to 0.09 μM), as indicated in Table **2**. The least amount of inhibitory activity was displayed by 1-hexyl- and 1-octyl substituted adamantane guanylhydrazones **G6** and **G7**, respectively, whose median effective concentration was above 6 μM. 1-Decyl substitution provided the most potent analogue (**G8**) of this series, with an EC$_{50}$ value of 0.09 μM. Compared to its unsubstituted congener **G1** (EC$_{50}$ = 56.9 μM), **G8** was 632-fold more active. Larger alkyl groups

seem to reduce trypanocidal activity, given that the 1-tetradecyl substituted analogue **G9** (EC$_{50}$ = 0.84 µM) was 9 times less effective than **G8**. It is noteworthy that replacement of the C=NH of guanylhydrazone moiety by the C=S functional group, which resulted in thiosemicarbazones **G10** and **G11**, enhanced their activity compared to the structurally related analogues **G6** and **G9** (EC$_{50}$ **G10** = 2.81 µM; EC$_{50}$ **G11** = 0.42 µM).

Table 3 Activity of the 1-alkyloxy-2-guanylhydrazone adamantanes **G12** – **G18** and the 1-benzyloxy-2-guanylhydrazone adamantanes **G19** – **G21** against cultured bloodstream form *T. brucei* (pH 7.4) *in vitro*.

Cmpd	Structure	*T. brucei* EC$_{50}$ (µM) [a]	*T. brucei* EC$_{90}$ (µM) [a]
G12		Marginal activity	Marginal activity
G13		1.17 ± 0.13	1.61 ± 0.26
G14		Marginal activity	Marginal activity
G15		Marginal activity	Marginal activity
G16		0.70 ± 0.07	0.98 ± 0.37
G17		3.64 ± 0.07	4.94 ± 0.05
G18		3.62 ± 0.28	4.91 ± 0.36
G19		1.84 ± 0.16	2.42 ± 0.08
G20		Marginal activity	Marginal activity

		T. brucei EC$_{50}$ (μM) ^{a}	T. brucei EC$_{90}$ (μM) ^{a}
G21		1.78 ± 0.17	3.88 ± 0.33

^{a} *Concentrations required to inhibit growth of T. brucei by 50% and 90%, respectively. EC$_{50}$ and EC$_{90}$ data are the mean of triplicate experiments ± SEM.*

Table **3** presents the results of the biological evaluation of the Series 3 analogues, 1-alkyloxy and 1-benzyloxy adamantane 2-guanylhydrazones (**G12** – **G21**). Most of them exhibited good trypanocidal activity, with potency in the range of 0.70-3.64 μM. The 1-hexyloxyethyl substituted adamantane **G12**, had a marginal activity towards *T. brucei*. Increasing the length of the alkyloxy chain of **G12** by only one carbon atom, resulting in derivative **G13** (heptyloxyethyl analogue), ~~appears to have~~ had a favorable effect on trypanocidal activity, resulting in an EC$_{50}$ of 1.17 μM. Somewhat surprisingly, further extension of the C1 alkyloxy side chain of **G13** by 1 or 3 carbon atoms (octyloxyethyl analogue **G14** and decyloxyethyl analogue **G15,** respectively) caused a reduction in activity. These biological results prompted the synthesis of homologue **G16,** whose trypanocidal activity was improved compared with **G13**, by shifting the oxygen atom from position 3 to position 4 of the side chain. Compound **G16** was the most potent of the mono(oxygenated) alkyl substituted adamantanes of this series, with an EC$_{50}$ value of 0.70 μM. The bis(oxygenated) ten-membered side chain substitution in analogue **G17** led to a slight decrease in activity, by 3 times with respect to the congener **G13** (EC$_{50}$ **G17** = 3.64 μM; EC$_{50}$ **G13** = 1.17 μM). Increasing the distance between the two oxygen atoms (from 2 to 5 carbons) gave rise to compound **G18**, which was equipotent to **G17** (approximately 3.6 μM). The same trend was observed for the three benzyl ethers **G19** – **G21,** which were either active in the low micromolar range, or inactive. More specifically, the benzyloxyethyl analogue **G20** showed a marginal activity. On the other hand, incorporation of a methylene and a 3-carbon propylene linker between the oxygen atom and the adamantane component, in analogues **G19** and **G21**, had an opposite effect. The resulting EC$_{50}$s were 1.84 μM and 1.78 μM, respectively.

Table 4 Activity of the aromatic-substituted 2-guanylhydrazone adamantanes **G22 – G25** against cultured bloodstream form *T. brucei* (pH 7.4) *in vitro*.		
Cmpd	**Structure**	*T. brucei* EC$_{50}$ (μM) ^{a}	*T. brucei* EC$_{90}$ (μM) ^{a}

G22		2.12 ± 0.09	2.81 ± 0.03
G23		0.41 ± 0.06	0.47 ± 0.01
G24		1.22 ± 0.17	2.48 ± 0.17
G25		2.06 ± 0.13	4.08 ± 0.13
[a] *Concentrations required to inhibit growth of T. brucei by 50% and 90%, respectively. EC_{50} and EC_{90} data are the mean of triplicate experiments ± SEM.*			

Activity of the aromatic 1-phenyl- or 1-benzyl- substituted 2-guanylhydrazone adamantanes **G22** – **G25** of Series 4 against cultured bloodstream form *T. brucei* (pH 7.4) *in vitro*, is presented in Table **4**. Aromatic substituted analogues **G22** – **G25** were active in the low micromolar range, with EC_{50} values between 0.41 μM and 2.12 μM. More specifically, phenyl substitution on the C-1 atom of the parent compound **G1** led to a 27-fold increase in potency of analogue **G22** (EC_{50} = 2.12 μM). Increasing the distance between the adamantane scaffold and the aromatic ring with a methylene group in compound **G23** ~~appears to~~ conferred a beneficial effect on trypanocidal activity. The EC_{50} value of **G23** (EC_{50} = 0.41 μM) was 5 times lower than that of **G22**. Introduction of the fluorine electron withdrawing group, in the *para*-position of the aromatic nucleus in analogue **G24**, slightly decreased activity (EC_{50} = 1.22 μM). The presence of the methoxy electron donating group at the same position had a similar effect. The EC_{50} of **G25** (2.06 μM) was increased by 1.7- and 5-fold compared to analogues **G24** and **G23**, respectively.

Table 5 Activity of the novel guanylhydrazone analogues **G26** – **G31** tested *in vitro* against cultured bloodstream form *T. brucei* (pH 7.4) and *T. cruzi* epimastigotes. Cytotoxicity against cultured rat skeletal myoblast L6 cells and selectivity indices.

Cmpd	Structure	T. brucei EC$_{50}$ (μM) [a]	T. brucei EC$_{90}$ (μM) [a]	SI T. brucei [b]	T. cruzi EC$_{50}$ (μM) [a]	T. cruzi EC$_{90}$ (μM) [a]	SI T. cruzi [b]	L6 cells CC$_{50}$ (μM) [c]
G26		1.62 ± 0.06	2.16 ± 0.02	-	-	-	-	-
G27		1.35 ± 0.09	1.71 ± 0.02	3.4	5.40 ± 1.17	11.2 ± 1	0.9	4.65 ± 0.54
G28		1.99 ± 0.06	2.72 ± 0.12	6.5	3.47 ± 0.15	4.90 ± 0.12	3.7	12.9 ± 0.3
G29		6.88 ± 0.72	13.1 ± 0.7	3.7	6.14 ± 0.33	11.6 ± 0.3	4.2	25.5 ± 0.6
G30		>30	-	-	>30	-	-	-
G31		14.3 ± 1.2	21.1 ± 0.6	13	>30	-	-	186 ± 11
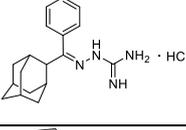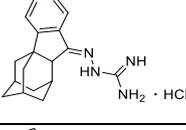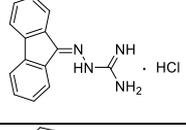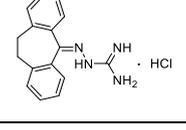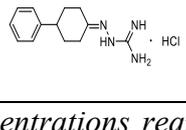
[a] Concentrations required to inhibit growth of T. brucei and T. cruzi by 50% and 90%, respectively. EC$_{50}$ and EC$_{90}$ data are the mean of triplicate experiments ± SEM. [b] Selectivity indices were calculated as the ratio of the CC$_{50}$ for L6 cells to EC$_{50}$ for T. brucei or T. cruzi, respectively. [c] Cytotoxicity was determined by establishing the concentration required to inhibit growth of cultured L6 cells by 50% (CC$_{50}$). Data are the mean of triplicate experiments ± SEM.

The novel analogues **G26 – G31** were tested for their trypanocidal potency against both cultured bloodstream form *T. brucei* and *T. cruzi* epimastigotes *in vitro*. The resulting EC$_{50}$ and EC$_{90}$ values are presented in Table **5**. Cytotoxicity values (CC$_{50}$) and selectivity indices (SIs) were also determined. The compounds bearing an adamantane core (**G26** – **G28**) were the most active, being in the low micromolar range, while the replacement of the adamantane scaffold led to compounds with decreased potency, in a higher micromolar level, with the exception of compound **G30**, which was inactive. More specifically, compounds **G26** – **G29** and **G31** exhibited considerable activity against *T. brucei* with EC$_{50}$ values ranging from 1.35 to 14.3 μM. With the **G26** analogue, the guanylhydrazone group was shifted in the methylene carbon of the benzyl substituent, with respect to the parent compound **G23**. This structural modification resulted in a higher EC$_{50}$ value by 4 times (EC$_{50}$ **G26** = 1.62 μM; EC$_{50}$ **G23** = 0.41 μM). The respective 2-substituted analogue **G27** was

equipotent to **G26** (EC$_{50}$ **G27** = 1.35 μM). Ring closure by formation of the C1 – C2' bond of **G27** resulted in the adamantane-cyclopentane-benzene fused analogue **G28**, which exhibited a similar inhibitory activity (EC$_{50}$ **G28** = 1.99 μM). Replacing the adamantane component with a second benzene ring lowered the activity ~~observed for~~ of the analogue **G29** by 3.5 fold (EC$_{50}$ **G29** = 6.88 μM), while changing the linker cyclopentane ring to the bulkier cycloheptane in compound **G30** abolished the activity. Finally, the use of a completely different and non-rigid scaffold, ~~like the one of~~ such as the 4-phenyl cyclohexane (**G31**), seems to compromise ~~disfavor~~ activity compared to the structurally related analogue **G29**, as **G31** was 2-fold less effective.

Most of the newly synthesized compounds were also tested against *T. cruzi* epimastigotes. Derivatives **G27**, **G28** and **G29** were the most potent, with EC$_{50}$ values being 5.40 μM, 3.47 μM and 6.14 μM, respectively. On the other hand, **G30** and **G31** showed no inhibition *in vitro* at 30 μM, which was the highest concentration tested. The cytotoxicity of the target compounds against mammalian cells was determined using the rat skeletal myoblast L6 cell line. The CC$_{50}$ values ranged between 4.65 for analogue **G27** and 186 μM for **G31**. Moreover, selectivity indices observed for *T. brucei* were generally higher than those observed for *T. cruzi*, as shown in Table **5**.

3.3 Computational studies

S-Adenosylmethionine Decarboxylase

Recently, Volkov and colleagues [157] elucidated the crystal structure of the *T. brucei* AdoMetDC/prozyme heterodimer in complex with a carbonimidic dihydrazide derivative well-known for its AdoMetDC inhibition activity, namely CGP 40215 (CGP) [108]. Structural data from the binding site of the protein-ligand complex reveal that CGP forms several interactions, including a bidentate H-bond with E266 and monodentate H-bonds with the backbone carbonyl of L83, the side chain hydroxyls of S249 and Y243, and with C100. Additionally, CGP is further stabilized through π-π stacking between Y243 and F28, as well as cation-π interactions with F28 (Fig. (**6**)). Due to the structural similarity of CGP with our guanylhydrazone analogues, it was thus hypothesized that both will share a common binding pattern, rendering these as interesting and novel in drug development for AdoMetDC. In order to test this hypothesis, *in silico* docking experiments were conducted. Furthermore, guanylhydrazone compound characterisation and model validation was obtained through an extended SAR and QSAR analysis.
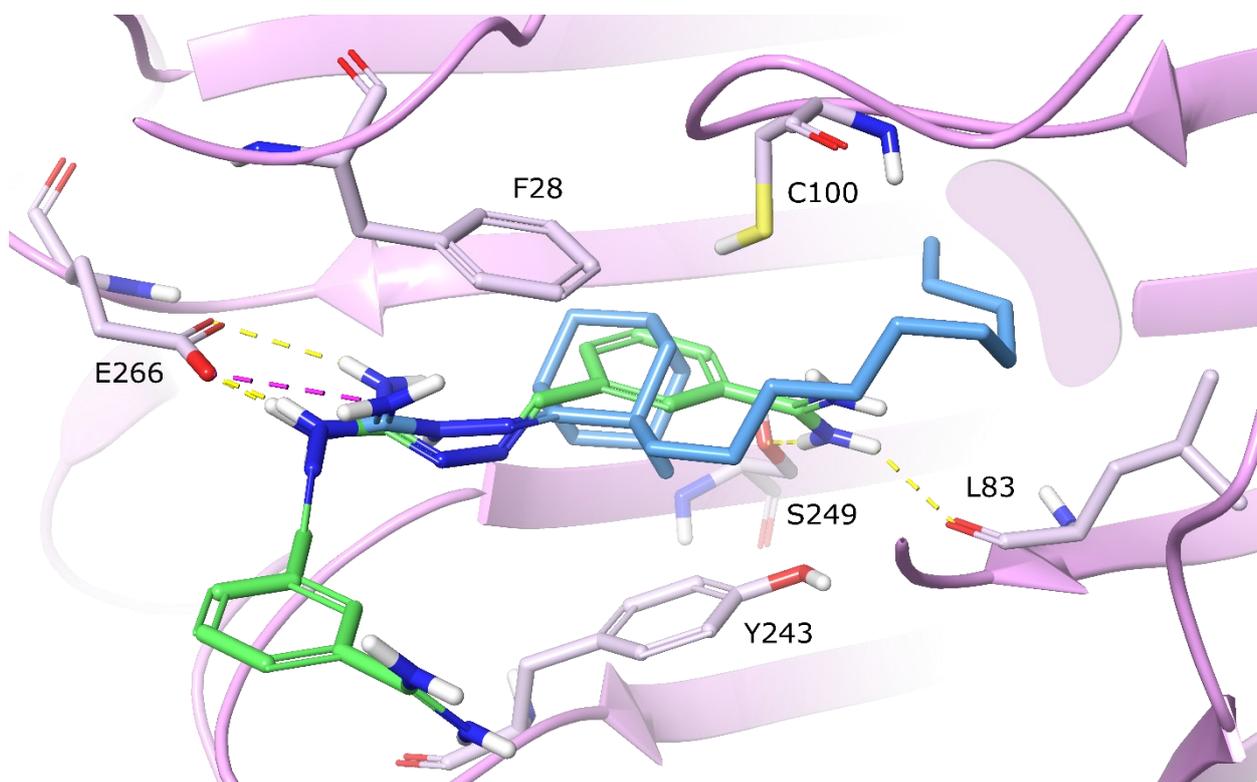
Fig. (6). Superposition of CGP and docking-fitted guanylhydrazone analogue **G8** within the AdoMetDC active site. The computationally cleaved three-dimensional crystal structure of *T. brucei* AdoMetDC (PDB: 5TVF) is shown in "ribbon" representation, colored in pink. Selected important residues contributing to various interactions are highlighted in "stick" representation. The pink "bean"-like shape on the right, symbolizes the hydrophobic cavity of AdoMetDC oriented towards the back of the binding site. CGP, the compound co-crystalized with AdoMetDC, is colored in green and the nanomolar range *T. brucei* inhibitor, guanylhydrazone analogue **G8**, is shown in light blue. Intriguingly, the positions of benzene and adamantane groups of CGP and **G8**, respectively, coincide and both compounds share common binding patterns with E266, as illustrated. CGP is further stabilized through two more hydrogen bonds with S249 and L83. Observed π-π stacking between Y243/F28 and cation-π interactions with F28, for CGP are not depicted in this figure.

Results of Docking-based scoring

Docking results shed light on the binding pattern of the guanylhydrazone analogues, which exhibit high resemblance ~~compared~~ to the crystal structure of the AdoMetDC and CGP complex, as shown in Fig. (**6**). Generally, all analogues form mono- and/or bidentate H-bonds through their guanyl group, either with E266 or with C246, and a minority of them with L83 or E85. Remarkably, the aliphatic side chains (that substitute the adamantane group) of some analogues stay inside the active site of

AdoMetDC in top-ranked poses scored within the broader 15 × 15 × 15 Å generated grid. However, this was not the case with the 10 × 10 × 10 Å grid, which seemingly impelled steric clashes with all lipophilic side chains due to space confinement. Therefore, the novel analogues **G26** – **G28** (Fig. (**7A**)) ranked on top even though their *T. brucei* activity proves otherwise. Due to this observation, all subsequent studies were performed within the broader grid.
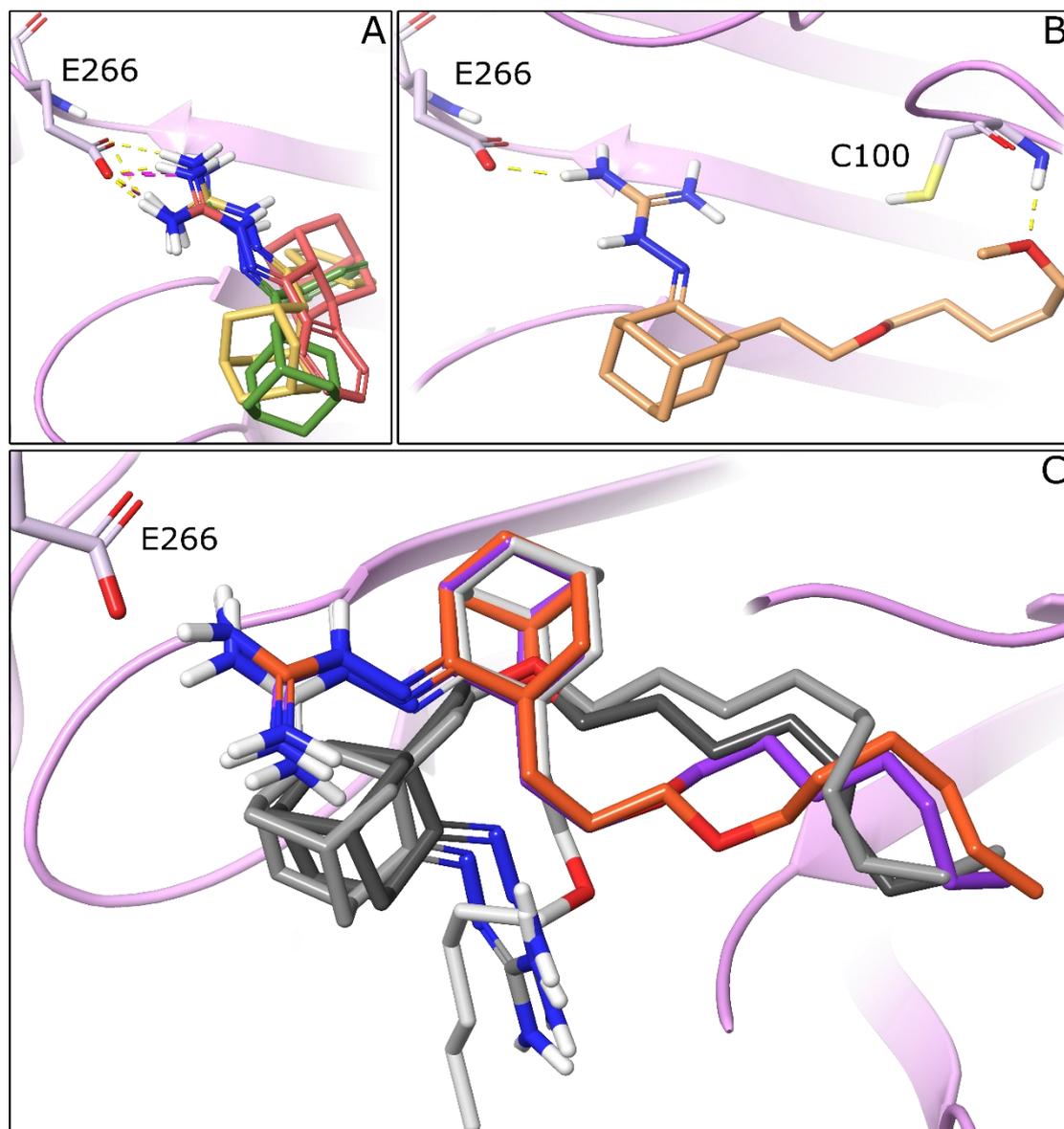
Fig. (7). Docking results for several guanylhydrazone analogues. A) Guanylhydrazone analogues **G26** (pale green), **G27** (pale yellow) and **G28** (pale red), three novel low micromolar *T. brucei* inhibitors, share identical polar interaction with E266 and position within the AdoMetDC active site, hence their minor activity variance. B) The binding profile of dietheric guanylhydrazone analogue **G18** (copper yellow). Formation of an intramolecular H-bond probably does not occur, due to stabilization *via* hydrogen bond with C100. Similar interactions

are observed for dietheric analogue **G17**. C) Superposition of guanylhydrazone analogues: **G12** (white), **G16** (orange), **G13** (purple), **G14** (dark grey) and **G15** (light grey). Active analogues **G16** and **G13** exhibit indistinguishable binding patterns, in contrast to the inactive analogue **G12**, which despite forming an H-bond with E266 of AdoMetDC, its large aliphatic group bolts towards the bulk of the solvent. Inactive analogues **G14** and **G15** score amongst the bottom ranks in docking due to the lack of polar interactions with AdoMetDC, in addition to the "false" orientation within the active site; the hydrophilic guanylhydrazone group faces towards the solvent and the hydrophobic adamantane group proximates polar E266.

Note that the substitution of the adamantane group at the *β*-position of the etheric oxygen (**G12**, **G14**, **G15** and **G20**) eliminates the activity when compared to the *α*- and *γ*- position (**G19** and **G16**, **G21** respectively), with the exception of analogue **G13** and the dietheric analogues **G17** and **G18**. This unexpected bioactivity result was further scrutinized by using molecular mechanics simulations, which yielded a high possibility of intramolecular H-bond formation between the etheric oxygen and the guanyl-group nitrogen, hence reduction in the *in vitro* activity. However, this was not applicable to the analogue **G13**. Furthermore, docking structural data show that the aliphatic chain of **G12** is placed outside of the AdoMetDC active site, resulting in ~~the~~ a lack of activity. Additionally, as illustrated in Fig. (**7C**), analogues **G14** and **G15** exhibit a dissimilar binding pattern to that previously described, with the guanylhydrazone group oriented towards the bulk of the solvent. Thus, no polar interactions with the protein are made and the activity becomes marginal. In contrast, dietheric analogues **G17** and **G18** exhibit *T. brucei* inhibitory activity, probably due to the second etheric oxygen interacting with AdoMetDC *via* an H-bond with the backbone of Cys100 (Fig. (**7B**)).

Docking-based structural data also failed to provide a rationale regarding the SAR analysis on slight side-chain differentiations among guanylhydrazone analogues. For instance, amongst the analogues **G6** – **G9** (of which **G8**, with a 10-carbon aliphatic chain, is the most potent guanylhydrazone inhibitor), analogue **G9**, with a 14C substitution, displays slightly diminished activity compared to **G8**. This outcome, could be termed, paraphrasing Schönherr and Cernak [158], as the "magic ethyl effect". It is therefore possible that reliance on solely docking-based approaches could be insufficient to interpret the SAR. As an alternative, a thermodynamic-driven approach was therefore implemented.

The thermodynamics of binding is influenced by multiple factors, including hydrogen bonding, hydrophobic interactions, protein and ligand rigidification, as well as the solvation and desolvation effect [159]. Therefore, avoiding a linearly correlated rule of thumb approach is vital when attempting to interpret binding affinity data. Even though H-bonds in theory favour enthalpy, hydrophobic

interactions favor entropy and conformational changes are unfavorable for entropy. One needs to consider that enthalpy and entropy of an intricate molecular system are vaguely interconnected. The theory of Enthalpy−Entropy Compensation (EEC) [160,161], which states that the enthalpy gain of a rigid protein-ligand complex is compensated by an entropy loss caused by the decrease of the available states for the system, provides partial explanation. However, as Wienen-Schmidt and colleagues showed, this is not always the case. Highest flexibility ligands can display, counterintuitively, the entropically most favored binding. Thus, the loss of degrees of freedom of the ligand does not necessarily monopolize the thermodynamic profile [162]. Adequate explanation for this unexpected thermodynamic outcome could be offered by the role of water molecules, which also strongly affect protein and ligand stability through their dipolar nature and the entropic gain associated with the hydrophobic effect [163]. Water molecules of the protein-ligand complex can be classified on the basis of their energetics into either high energy, unstable water molecules trapped inside hydrophobic cavities or stable water molecule that are stabilized through extensive interactions with the protein over the corresponding solvent accessible surface [164]. Computational tools such as SZmap [165] from Openeye, have been used to incorporate the water network in drug design. SZmap (solvent-Zap-mapping) is capable of quantitatively predicting water positions and their energetics, and is potentially a useful tool for identifying significant favorable or unfavorable regions of solvent thermodynamics in the binding site [166]. The hydration analysis *via* SZmap for the active site of AdoMetDC was performed as previously described [167] and the results were visually inspected.

Predictably, SZmap solvation mapping analysis yielded interesting results that compensated for the limitations of a merely docking-scoring approach. The binding site of AdoMetDC is rich in both stable and unstable water molecules, which through their displacement influence binding thermodynamics. Since all analogues are comprised of bulky hydrophobic groups, such as aliphatic hydrocarbons, adamantane and benzene moieties, water molecules are inevitably displaced. With the introduction of the polar guanylhydrazone group, which ideally contributes to favorable enthalpy *via* structural water molecule displacement, elucidating the complete thermodynamic binding profile becomes complex. Specifically, for **G8**, a nanomolar-range *T. brucei* inhibitor, SZmap data showed that the adamantane group as well as the 10C side chain displace unstable, high-energy water molecules (Fig. (**8**)), thus contributing to the increase of entropy.
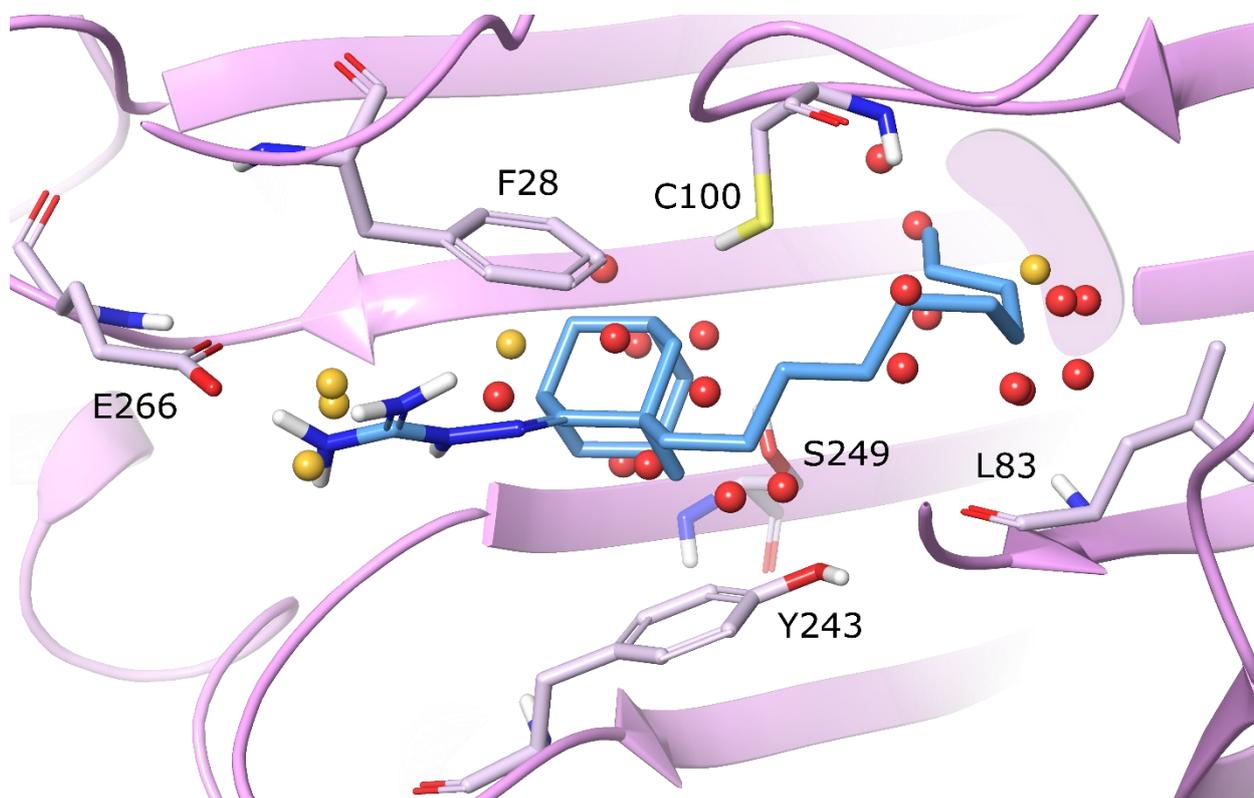
Fig. (8). SZmap-generated hydration analysis of the active site of AdoMetDC with docking-fitted **G8** analogue. The red spheres define the high energy water molecules, while gold spheres depict structural water molecules. Selected amino acids are illustrated for viewing reference. The inhibitor is oriented so as to position both hydrophobic adamantane and 10-carbon aliphatic groups towards unstable water molecules, thus permitting their displacement and leading to affinity enhancement due to favorable entropic contributions. The polar guanylhydrazone group thereby provokes the displacement of three highly stable water molecules, from the hydration site adjacent to E266, and the enthalpic effect is pronounced.

In contrast, the guanylhydrazone group displaces low energy structural water molecules and therefore adds to the enthalpic effect. Hydration data for analogue **G9** show a contiguity, with the exception of the adamantane group, which does not displace water molecules in this context. Apparently, this guanylhydrazone analogue poorly docks within the active site of AdoMetDC. Therefore, a displacement of three stable water molecules by the adamantane group would occur, resulting in enthalpic cost, which conceivably eliminates the activity against *T. brucei*. Analogous interpretation of the displacement of high/low energy water molecules by polar or hydrophobic groups can also be made for other guanylhydrazone analogues of similar structure, but different activity (**G10** and **G11**;

G24 and **G25**; **G2** and **G3**). These differences could be related to EEC and should be further investigated.

Results of QSAR analysis

All statistical methods comprised of only the active analogues yielded substantial model fidelity, based on their statistical properties, as illustrated in Table **6**.

Table 6. Statistical values of Multiple Linear Regression (MLR), Partial Least Squares regression (PLS) and Kernel-based Partial Least Squares regression (KPLS) regression models.

Statistical Regression Model	Training set	Test set	R^2	Q^2	SD	RMSE
MLR	22	5	0.9339	0.8270	0.2510	0.3569
PLS	22	5	0.8890	0.3573	0.3350	0.5466
KPLS	22	5	0.9662	0.9105	0.1752	0.2922

Interestingly, the most accurate regression model was generated through KPLS ($R^2 = 0.9662$; $Q^2 = 0.9105$). PLS had less predictive accuracy ($R^2 = 0.8890$; $Q^2 = 0.3575$). MLR analysis also produced an acceptable model ($R^2 = 0.9339$; $Q^2 = 0.8270$). However, it was challenged by notable inter-correlation within the Canvas-derived optimal subset of descriptors, thus rendering the respective MLR model as one of limited predicting capacity. Out of the molecular descriptors identified as significant by the statistical analysis, the most meaningful were the following; average vertex distance degree, Balaban distance connectivity index, conformation independent QPlogS, Gutman molecular topological and topological charge index of order 9. Details ~~description~~ of these descriptors can be acquired from the Handbook of Molecular Descriptors, by Todeschini and colleagues [168]. Fundamentally, molecular descriptors, due to the involvement of mathematics, usually lack direct structural interpretation of a molecule. Since chemical information is transformed through various procedures into sole numeric values, deducing tangible characteristics about the structure of a compound is rather difficult. That said, it is important to construct a reliable and highly predictable model, regardless of its ability to interpret structural features. Such a model would enable rapid and accurate activity predictions, even for novel compounds currently non-synthesized, and provide proof-of-concept for further drug development approaches.

Experimental and predicted EC_{50} values of active guanylhydrazone analogues for *T. brucei* are shown in Table **7**.

Table 7. Statistical analysis comparison for the active guanylhydrazone analogues with Multiple Linear Regression (MLR), Partial Least Squares regression (PLS) and Kernel-based Partial Least Squares regression (KPLS). Experimental and predicted *T. brucei* inhibitory activity for only active guanylhydrazone analogues is presented. IC_{50} (μM) values are logarithmically converted and the absolute error is calculated. Error values are color-coded. As the absolute error approximates the numeric value of one, activity shifts one order of magnitude.

Active Compounds	Activity ($-logIC_{50}$, M)	MLR		PLS		KPLS	
		Pred(Activity) ($-logIC_{50}$, M)	Abs Error	Pred(Activity) ($-logIC_{50}$, M)	Abs Error	Pred(Activity) ($-logIC_{50}$, M)	Abs Error
G1	4.245	4.4286	0.184	4.3413	0.096	4.264	0.019
G2	3.777	3.7012	0.076	3.8435	0.066	3.701	0.076
G3	5.015	4.8865	0.128	3.9843	1.030	5.145	0.130
G4	3.523	3.5935	0.071	3.4518	0.071	3.789	0.266
G5	3.523	3.9734	0.451	3.4956	0.027	3.541	0.018
G6	5.222	5.0027	0.219	5.5995	0.378	5.225	0.003
G7	5.222	5.9432	0.721	5.9604	0.738	5.483	0.261
G8	7.046	6.6705	0.375	6.3055	0.741	6.525	0.521
G9	6.076	5.9545	0.122	6.7108	0.635	6.224	0.148
G10	5.551	5.5515	0.000	5.3923	0.159	5.396	0.155
G11	6.377	6.5462	0.169	6.4279	0.051	5.880	0.497
G13	5.932	6.0622	0.130	5.8398	0.092	6.049	0.117
G16	6.155	6.0622	0.093	5.8456	0.309	6.242	0.087
G17	5.439	5.4502	0.011	5.4164	0.023	5.404	0.035
G18	5.441	5.4502	0.009	5.3975	0.043	5.318	0.123
G19	5.735	5.9315	0.196	5.8350	0.100	5.771	0.036
G21	5.75	5.8070	0.057	6.0994	0.349	5.919	0.169
G22	5.674	5.6424	0.032	5.7052	0.031	5.697	0.023
G23	6.387	6.1335	0.254	5.9330	0.454	6.417	0.030
G24	5.914	5.9296	0.016	5.9442	0.030	5.896	0.018
G25	5.686	5.5693	0.117	5.8503	0.164	5.730	0.044
G26	5.790	5.9990	0.209	5.8412	0.051	5.951	0.161
G27	5.870	6.1250	0.255	5.9097	0.040	5.858	0.012

G28	5.701	5.6679	0.033	5.7783	0.077	5.590	0.111
G29	5.162	4.9830	0.179	4.8028	0.360	5.082	0.080
G30	4.523	4.5656	0.043	4.7354	0.213	4.407	0.116
G31	4.845	5.4141	0.569	4.8898	0.045	5.069	0.224

As can be observed, all three regression models yielded medium to relatively high absolute error values for analogues **G7** and **G8**. A possible explanation for this observation can be, again, related to the effect of the solvent. Software implementing the ligand-based drug discovery approach, such as Canvas, are exclusively focused on the ligand structure and can thus seriously neglect the exact thermodynamic effect that individual water molecules might have on the binding affinity of small molecules that can displace them. The displacement of water molecules affects each compound differently, hence the almost absolute agreement for analogues **G2**, **G17**, **G18**, **G22**, **G24** among all statistical approaches. Generated statistical data should be considered as a stepping-stone for further investigation.

Conclusion

In summary, the data obtained from this extended SAR study illustrate: (i) The synergistic effect of the lipophilic character of the C1 substitution and C2 guanylhydrazone moiety on trypanocidal activity. (ii) The critical role of the adamantane moiety for trypanocidal activity. Replacement of the adamantane cage structure by the tricyclic scaffolds of fluorene and dibenzocycloheptene, and the bendable 4-phenyl cyclohexane decreases activity against *T. brucei*. (iii) The great importance of the nature and length of the second substitution to antiparasitic activity. Replacement of the lipophilic alkyl chain at of the adamantane-based guanylhydrazones with a more polar component (alkyloxy, hydroxyl, aminoguanidine) results in a substantial reduction in trypanocidal properties. Finally, a number of diverse approaches were undertaken to understand the interplay between the structure of the promising bioactive compounds and the activity against their putative protozoan target, AdoMetDC. Chemoinformatics-based models afforded a series of molecular descriptors that might account for the observed bioactivity and sustain the design of new derivatives. In addition, molecular docking simulations, enhanced by a hydration analysis, derived interesting thermodynamic insights into the role of structural factors, such as intramolecular hydrogen bonding or displacement of energetically unfavorable water molecules on the observed binding affinity. The design of new compounds with improved bioactivity against AdoMetDC could greatly benefit from such rational approaches. Efforts towards this direction are currently underway.

LIST OF ABBREVIATIONS

3D : Three-dimensional

AdoMet : *S*-adenosylmethionine

AdoMetDC : *S*-adenosylmethionine decarboxylase

BBB : blood-brain barrier

BZ : benznidazole

CADD : Computer-aided drug design

CATT : card agglutination test for trypanosomiasis

CNS : central nervous system

CSF : cerebrospinal fluid

CC_{50} : half maximal cytotoxic concentration, concentration required to cause cytotoxic effect by 50% or to inhibit growth of cultured L6 cells by 50%

CGP : derivative CGP 40215 (AdoMetDC inhibitor)

DMF : *N,N*-dimethylformamide

DMSO : dimethyl sulfoxide

DRC : Democratic Republic of Congo

EC_{50} : half maximal effective concentration, concentration required to give half-maximal response or concentration required to inhibit growth of *T. brucei* and *T. cruzi* by 50%

EEC : Enthalpy−Entropy Compensation

Et_2O : diethyl ether

EtOH : ethanol

FBDD : Fragment-based drug discovery

gHAT : *gambiense* HAT

Gsp : glutathionylspermidine

HAT : Human African Trypanosomiasis

LBDD : Ligand-based drug design

IgM : Immunoglobulin M

IM : intramuscular

IV : intravenous

KPLS : Kernel-based Partial Least Squares

MLR : Multiple Linear Regression

NECT : nifurtimox-eflornithine combination treatment

NTDs : neglected tropical diseases

ODC : ornithine decarboxylase

PLS : Partial Least Squares

PTRE : post-treatment reactive encephalopathy

QSAR : Quantitative structure-activity relationship

rHAT : *rhodesiense* HAT

SBDD : Structure-based drug design

SD : Standard deviation

SI : selectivity index

SZMAP : solvent-Zap-mapping

T. brucei : *Trypanosoma brucei*

THF : tetrahydrofuran

VdW : van der Waals

WBC : white blood cells

WHO : World Health Organization

CONFLICT OF INTEREST

 There are no conflicts to declare.

CONSENT FOR PUBLICATION:

All the authors consent for this publication.

REFERENCES

[1] Mackey TK, Liang BA, Cuomo R, Hafen R, Brouwer KC, Lee DE. Emerging and reemerging neglected tropical diseases: a review of key characteristics, risk factors, and the policy and innovation environment. Clin Microbiol Rev 2014; 27(4): 949-79.

[2] Addisu A, Adriaensen W, Balew A, *et al*. Neglected tropical diseases and the sustainable development goals: an urgent call for action from the front line. BMJ Glob Health 2019; 4(1): e001334.

[3] Peeling RW, Boeras DI, Nkengasongb J. Re-imagining the future of diagnosis of Neglected Tropical Diseases. Comput Struct Biotechnol J 2017; 15: 271-4.

[4] Mitra AK, Mawson AR. Neglected Tropical Diseases: epidemiology and global burden. Trop Med Infect Dis 2017; 2(3): 36.

[5] Varikuti S, Jha BK, Volpedo G, *et al*. Host-directed drug therapies for Neglected Tropical Diseases caused by protozoan parasites. Front Microbiol 2018; 9: 2655.

[6] Hotez PJ, Kamath A. Neglected tropical diseases in sub-saharan Africa: review of their prevalence, distribution, and disease burden. PLoS Negl Trop Dis 2009; 3(8): e412.

[7] Kennedy PGE. Update on human African trypanosomiasis (sleeping sickness). J Neurol 2019; 266(9): 2334-37.

[8] World Health Organization, Trypanosomiasis, human African (sleeping sickness) [updated 2019 April 12; cited 2019 August]. Available from: (https://www.who.int/news-room/fact-sheets/detail/trypanosomiasis-human-african-(sleeping-sickness)).

[9] Bottieau E, Clerinx J. Human African Trypanosomiasis: progress and stagnation. Infect Dis Clin North Am 2019; 33(1): 61-77.

[10] Büscher P, Cecchi G, Jamonneau V, Priotto G. Human African trypanosomiasis. Lancet 2017; 390(10110): 2397-2409.

[11] Malvy D, Chappuis F. Sleeping sickness. Clin Microbiol Infect 2011; 17(7): 986-95.

[12] Geiger A, Ravel S, Mateille T, *et al*. Vector competence of *Glossina palpalis gambiensis* for *Trypanosoma brucei* s.l. and genetic diversity of the symbiont *Sodalis glossinidius*. Mol Biol Evol 2007; 24(1): 102-9.

[13] Geiger A, Cuny G, Frutos R. Two tsetse fly species, *Glossina palpalis gambiensis* and *Glossina morsitans morsitans*, carry genetically distinct populations of the secondary symbiont *Sodalis glossinidius*. Appl Environ Microbiol 2005; 71(12): 8941-3.

[14] Steverding D. The history of African trypanosomiasis. Parasit Vectors 2008; 1(1): 3.

[15] Welburn SC, Molyneux DH, Maudlin I. Beyond tsetse--implications for research and control of Human African Trypanosomiasis epidemics. Trends Parasitol 2016; 32(3): 230-41.

[16] Kennedy PGE, Rodgers J. Clinical and neuropathogenetic aspects of Human African Trypanosomiasis. Front Immunol 2019; 10: 39.

[17] Franco JR, Cecchi G, Priotto G, *et al*. Monitoring the elimination of human African trypanosomiasis: Update to 2016. PLoS Negl Trop Dis 2018; 12(12): e0006890.

[18] Franco JR, Simarro PP, Diarra A, Jannin JG. Epidemiology of human African trypanosomiasis. Clin Epidemiol 2014; 6: 257-75.

[19] Lindner AK, Priotto G. The unknown risk of vertical transmission in sleeping sickness--a literature review. PLoS Negl Trop Dis 2010; 4(12): e783.

[20] Gaillot K, Lauvin MA, Cottier JP. Vertical transmission of human African trypanosomiasis: Clinical evolution and brain MRI of a mother and her son. PLoS Negl Trop Dis 2017; 11(7): e0005642.

[21] Biteau N, Asencio C, Izotte J, *et al*. *Trypanosoma brucei gambiense* Infections in mice lead to tropism to the reproductive organs, and horizontal and vertical transmission. PLoS Negl Trop Dis 2016; 10(1): e0004350.

[22] Rocha G, Martins A, Gama G, Brandão F, Atouguia J. Possible cases of sexual and congenital transmission of sleeping sickness. Lancet. 2004; 363(9404): 247.

[23] Migchelsen SJ, Büscher P, Hoepelman AI, Schallig HD, Adams ER. Human African trypanosomiasis: a review of non-endemic cases in the past 20 years. Int J Infect Dis 2011; 15(8): e517-24.

[24] Kennedy PGE. Clinical features, diagnosis, and treatment of human African trypanosomiasis (sleeping sickness). Lancet Neurol 2013; 12(2): 186-94.

[25] Chappuis F, Loutan L, Simarro P, Lejon V, Büscher P. Options for field diagnosis of human african trypanosomiasis. Clin Microbiol Rev 2005; 18(1): 133-46.

[26] Kennedy PGE, Human African trypanosomiasis of the CNS: current issues and challenges. J Clin Invest 2004; 113(4): 496-504.

[27] Checchi F, Funk S, Chandramohan D, Haydon DT, Chappuis F. Updated estimate of the duration of the meningo-encephalitic stage in gambiense human African trypanosomiasis. BMC Res Notes 2015; 8: 292.

[28] Mogk S, Boßelmann CM, Mudogo CN, Stein J, Wolburg H, Duszenko M. African trypanosomes and brain infection - the unsolved question. Biol Rev Camb Philos Soc 2017; 92(3): 1675-87.

[29] Njamnshi AK, Gettinby G, Kennedy PGE. The challenging problem of disease staging in human African trypanosomiasis (sleeping sickness): a new approach to a circular question. Trans R Soc Trop Med Hyg 2017; 111(5): 199-203.

[30] Bonnet J, Boudot C, Courtioux B. Overview of the diagnostic methods used in the field for Human African Trypanosomiasis: what could change in the next years? Biomed Res Int 2015; 2015: 583262.

[31] Büscher P, Mertens P, Leclipteux T, *et al*. Sensitivity and specificity of HAT Sero-K-SeT, a rapid diagnostic test for serodiagnosis of sleeping sickness caused by *Trypanosoma brucei gambiense*: a case-control study. Lancet Glob Health 2014; 2(6): e359-63.

[32] Ponte-Sucre A. An overview of *Trypanosoma brucei* infections: an intense host-parasite interaction. Front Microbiol 2016; 7: 2126.

[33] Kato CD, Matovu E, Mugasa CM, Nanteza A, Alibu VP. The role of cytokines in the pathogenesis and staging of *Trypanosoma brucei rhodesiense* sleeping sickness. Allergy Asthma Clin Immunol 2016; 12: 4.

[34] Barrett MP, Boykin DW, Brun R, Tidwell RR. Human African trypanosomiasis: pharmacological re-engagement with a neglected disease. Br J Pharmacol 2007; 152(8): 1155-71.

[35] Steverding D. Sleeping Sickness and Nagana Disease Caused by *Trypanosoma brucei*. In: Marcondes C, Eds. Arthropod Borne Diseases. Cham: Springer 2017; pp. 277-97.

[36] Babokhov P, Sanyaolu AO, Oyibo WA, Fagbenro-Beyioku AF, Iriemenam NC. A current analysis of chemotherapy strategies for the treatment of human African trypanosomiasis. Pathog Glob Health 2013; 107(5): 242-52.

[37] Thomas JA, Baker N, Hutchinson S, *et al*. Insights into antitrypanosomal drug mode-of-action from cytology-based profiling. PLoS Negl Trop Dis 2018; 12(11): e0006980.

[38] Zhang Y, Li Z, Pilch DS, Leibowitz MJ. Pentamidine inhibits catalytic activity of group I intron Ca.LSU by altering RNA folding. Nucleic Acids Res 2002; 30(13): 2961-71.

[39] Jacobs RT, Nare B, Phillips MA. State of the art in African trypanosome drug discovery. Curr Top Med Chem 2011; 11(10): 1255-74.

[40] Denise H, Barrett MP. Uptake and mode of action of drugs used against sleeping sickness. Biochem Pharmacol 2001; 61(1): 1-5.

[41] Franco JR, Simarro PP, Diarra A, Ruiz-Postigo JA, Samo M, Jannin JG. Monitoring the use of nifurtimox-eflornithine combination therapy (NECT) in the treatment of second stage gambiense human African trypanosomiasis. Res Rep Trop Med 2012; 3: 93-101.

[42] Eperon G, Balasegaram M, Potet J, Mowbray C, Valverde O, Chappuis F. Treatment options for second-stage gambiense human African trypanosomiasis. Expert Rev Anti Infect Ther 2014; 12(11): 1407-17.

[43] Kansiime F, Adibaku S, Wamboga C. A multicentre, randomised, non-inferiority clinical trial comparing a nifurtimox-eflornithine combination to standard eflornithine monotherapy for late stage

Trypanosoma brucei gambiense human African trypanosomiasis in Uganda. Parasit Vectors 2018; 11(1): 105.

[44] Deeks ED. Fexinidazole: first global approval. Drugs 2019; 79(2): 215-220.

[45] Chappuis F. Oral fexinidazole for human African trypanosomiasis. Lancet 2018; 391(10116): 100-102.

[46] Baker CH, Welburn SC. The long wait for a new drug for Human African Trypanosomiasis. Trends Parasitol 2018; 34(10): 818-27.

[47] Nagle AS, Khare S, Kumar AB, *et al*. Recent developments in drug discovery for leishmaniasis and human African trypanosomiasis. Chem Rev 2014; 114(22): 11305-47.

[48] Steketee PC, Vincent IM, Achcar F, *et al*. Benzoxaborole treatment perturbs *S*-adenosyl-L-methionine metabolism in *Trypanosoma brucei*. PLoS Negl Trop Dis 2018; 12(5): e0006450.

[49] Lewis MD, Francisco AF, Jayawardhana S, Langston H, Taylor MC, Kelly JM. Imaging the development of chronic Chagas disease after oral transmission. Sci Rep 2018; 8(1): 11292.

[50] World Health Organization, Chagas disease (American trypanosomiasis). [updated 2019 April 17; cited 2019 August]. Available from: https://www.who.int/en/news-room/fact-sheets/detail/chagas-disease-(american-trypanosomiasis).

[51] Pérez-Molina JA, Perez AM, Norman FF, Monge-Maillo B, López-Vélez R. Old and new challenges in Chagas disease. Lancet Infect Dis 2015; 15(11): 1347-56.

[52] Stevens L, Dorn PL, Schmidt JO, Klotz JH, Lucero D, Klotz SA. Kissing bugs. The vectors of Chagas. Adv Parasitol 2011; 75: 169-92.

[53] Rassi A Jr, Rassi A, Marin-Neto JA. Chagas disease. Lancet 2010; 375(9723): 1388-1402.

[54] Rajão MA, Furtado C, Alves CL, *et al*. Unveiling benznidazole's mechanism of action through overexpression of DNA repair proteins in *Trypanosoma cruzi*. Environ Mol Mutagen 2014; 55(4): 309-21.

[55] Bermudez J, Davies C, Simonazzi A, Real JP, Palma S. Current drug therapy and pharmaceutical challenges for Chagas disease. Acta Trop 2016; 156: 1-16.

[56] Field MC, Horn D, Fairlamb AH, *et al*. Anti-trypanosomatid drug discovery: an ongoing challenge and a continuing need. Nat Rev Microbiol 2017; 15(7): 447.

[57] Stich A, Ponte-Sucre A, Holzgrabe U. Do we need new drugs against human African trypanosomiasis? Lancet Infect Dis 2013; 13(9): 733-4.

[58] Willert E, Phillips MA. Regulation and function of polyamines in African trypanosomes. Trends Parasitol 2012; 28(2): 66-72.

[59] Phillips MA. Polyamines in protozoan pathogens. J Biol Chem 2018; 293(48): 18746-56.

[60] Müller S, Coombs GH, Walter RD. Targeting polyamines of parasitic protozoa in chemotherapy. Trends Parasitol 2001; 17(5): 242-9.

[61] Keiser J, Stich A, Burri C. New drugs for the treatment of human African trypanosomiasis: research and development. Trends Parasitol 2001; 17(1): 42-9.

[62] Heby O, Persson L, Rentala M. Targeting the polyamine biosynthetic enzymes: a promising approach to therapy of African sleeping sickness, Chagas' disease, and leishmaniasis. Amino Acids 2007; 33(2): 359-66.

[63] Birkholtz LM, Williams M, Niemand J, Louw AI, Persson L, Heby O. Polyamine homoeostasis as a drug target in pathogenic protozoa: peculiarities and possibilities. Biochem J 2011; 438(2): 229-44.

[64] Smithson DC, Lee J, Shelat AA, Phillips MA, Guy RK. Discovery of potent and selective inhibitors of *Trypanosoma brucei* ornithine decarboxylase. J Biol Chem 2010; 285(22): 16771-81.

[65] Tekwani BL, Bacchi CJ, Secrist JA 3rd, Pegg AE. Irreversible inhibition of *S*-adenosylmethionine decarboxylase of *Trypanosoma brucei brucei* by *S*-adenosylmethionine analogues. Biochem Pharmacol 1992; 44(5): 905-11.

[66] Hirth B, Barker RH Jr, Celatka CA, *et al*. Discovery of new *S*-adenosylmethionine decarboxylase inhibitors for the treatment of Human African Trypanosomiasis (HAT). Bioorg Med Chem Lett 2009; 19(11): 2916-9.

[67] Barker RH Jr, Liu H, Hirth B, *et al*. Novel *S*-adenosylmethionine decarboxylase inhibitors for the treatment of human African trypanosomiasis. Antimicrob Agents Chemother 2009; 53(5): 2052-8.

[68] Bacchi CJ, Barker RH Jr, Rodriguez A, *et al*. Trypanocidal activity of 8-methyl-5'-{[(Z)-4-aminobut-2-enyl]-(methylamino)}adenosine (Genz-644131), an adenosylmethionine decarboxylase inhibitor. Antimicrob Agents Chemother 2009; 53(8): 3269-72.

[69] Volkov OA, Cosner CC, Brockway AJ, *et al*. Identification of *Trypanosoma brucei* AdoMetDC inhibitors using a high-throughput mass spectrometry-based assay. ACS Infect Dis 2017; 3(7): 512-26.

[70] Volkov OA, Brockway AJ, Wring SA, *et al*. Species-selective pyrimidineamine inhibitors of *Trypanosoma brucei S*-adenosylmethionine decarboxylase. J Med Chem 2018; 61(3): 1182-203.

[71] Brockway AJ, Volkov OA, Cosner CC, *et al*. Synthesis and evaluation of analogs of 5'-(((Z)-4-amino-2-butenyl)methylamino)-5'-deoxyadenosine (MDL 73811, or AbeAdo) - An inhibitor of *S*-adenosylmethionine decarboxylase with antitrypanosomal activity. Bioorg Med Chem 2017; 25(20): 5433-40.

[72] Velez N, Brautigam CA, Phillips MA. *Trypanosoma brucei S*-adenosylmethionine decarboxylase N terminus is essential for allosteric activation by the regulatory subunit prozyme. J Biol Chem 2013; 288(7): 5232-40.

[73] Lamoureux G, Artavia G. Use of the adamantane structure in medicinal chemistry. Curr Med Chem 2010; 17(26): 2967-78.

[74] Wanka L, Iqbal K, Schreiner PR. The lipophilic bullet hits the targets: medicinal chemistry of adamantane derivatives. Chem Rev 2013; 113(5): 3516-604.

[75] Van der Schyf CJ, Geldenhuys WJ. Polycyclic compounds: ideal drug scaffolds for the design of multiple mechanism drugs? Neurotherapeutics 2009; 6(1): 175-86.

[76] Stockdale TP, Williams CM. Pharmaceuticals that contain polycyclic hydrocarbon scaffolds. Chem Soc Rev 2015; 44(21): 7737-63.

[77] Štimac A, Šekutor M, Mlinarić-Majerski K, Frkanec L, Frkanec R. Adamantane in drug delivery systems and surface recognition. Molecules 2017; 22(2): E297.

[78] Geldenhuys WJ, Malan SF, Bloomquist JR, Marchand AP, Van der Schyf CJ. Pharmacology and structure-activity relationships of bioactive polycyclic cage compounds: a focus on pentacycloundecane derivatives. Med Res Rev 2005; 25(1): 21-48.

[79] Liu J, Obando D, Liao V, Lifa T, Codd R. The many faces of the adamantyl group in drug design. Eur J Med Chem 2011; 46(6): 1949-63.

[80] Grillaud M, Bianco A. Multifunctional adamantane derivatives as new scaffolds for the multipresentation of bioactive peptides. J Pept Sci 2015; 21(5): 330-45.

[81] Horvat S, Mlinaric-Majerski K, Glavas-Obrovac L, *et al*. Tumor-cell-targeted methionine-enkephalin analogues containing unnatural amino acids: design, synthesis, and *in vitro* antitumor activity. J Med Chem 2006; 49(11): 3136-42.

[82] Li Z, Khaliq M, Zhou Z, Post CB, Kuhn RJ, Cushman M. Design, synthesis, and biological evaluation of antiviral agents targeting flavivirus envelope proteins. J Med Chem 2008; 51(15): 4660-71.

[83] Ajdačić V, Senerovic L, Vranić M, *et al*. Synthesis and evaluation of thiophene-based guanylhydrazones (iminoguanidines) efficient against panel of voriconazole-resistant fungal isolates. Bioorg Med Chem 2016; 24(6): 1277-91.

[84] Ajdačić V, Lazić J, Mojičević M, Šegan S, Nikodinović-Runić J, Opsenica I. Antibacterial and antifungal properties of guanylhydrazones. J Serb Chem Soc 2017; 82(6): 641-49.

[85] Gadad AK, Mahajanshetti CS, Nimbalkar S, Raichurkar A. Synthesis and antibacterial activity of some 5-guanylhydrazone/thiocyanato-6-arylimidazo[2,1-b]-1,3,4-thiadiazole-2-sulfonamide derivatives. Eur J Med Chem 2000; 35(9): 853-7.

[86] Bairwa R, Kakwani M, Tawari NR. Novel molecular hybrids of cinnamic acids and guanylhydrazones as potential antitubercular agents. Bioorg Med Chem Lett 2010; 20(5): 1623-5.

[87] Silva FP, Dantas BB, Faheina Martins GV, de Araújo DA, Vasconcellos ML. Synthesis and anticancer activities of novel guanylhydrazone and aminoguanidine tetrahydropyran derivatives. Molecules 2016; 21(6): E671.

[88] Andreani A, Burnelli S, Granaiola M, *et al*. Synthesis and antitumor activity of guanylhydrazones from 6-(2,4-Dichloro-5-nitrophenyl)imidazo[2,1-b]thiazoles and 6-Pyridylimidazo[2,1-b]thiazoles. J Med Chem 2006; 49(26): 7897-901.

[89] Kamal A, Kashi Reddy M, Viswanath A. The design and development of imidazothiazole-chalcone derivatives as potential anticancer drugs. Expert Opin Drug Discov 2013; 8(3): 289-304.

[90] de Oliveira CBJ, Neto DCF, de Almeida JSFD, *et al*. Synthesis of new quinoline-piperonal hybrids as potential drugs against Alzheimer's disease. Int J Mol Sci 2019; 20(16): 3944.

[91] Neto DCF, de Souza Ferreira M, da Conceição Petronilho E, *et al*. A new guanylhydrazone derivative as a potential acetylcholinesterase inhibitor for Alzheimer's disease: synthesis, molecular docking, biological evaluation and kinetic studies by nuclear magnetic resonance. RSC Adv 2017; 7: 33944-52.

[92] Soll RM, Lu T, Tomczuk B, *et al*. Amidinohydrazones as guanidine bioisosteres: application to a new class of potent, selective and orally bioavailable, non-amide-based small-molecule thrombin inhibitors. Bioorg Med Chem Lett 2000; 10(1): 1-4.

[93] Barron S, Lewis B, Wellmann K, *et al*. Polyamine modulation of NMDARs as a mechanism to reduce effects of alcohol dependence. Recent Pat CNS Drug Discov 2012; 7(2): 129-44.

[94] Kathuria D, Chourasiya SS, Wani AA, Singh M, Sahoo SC, Bharatam PV. Geometrical isomerism in guanabenz free base: synthesis, characterization, crystal structure, and theoretical studies. Cryst Growth Des 2019; 19(6): 3183-91.

[95] Wang J, Grishin AV, Ford HR. Experimental anti-inflammatory drug semapimod inhibits TLR signaling by targeting the TLR chaperone gp96. J Immunol 2016; 196(12): 5130-7.

[96] Pardali V, Giannakopoulou E, Konstantinidi A, Kolocouris A, Zoidis G. 1,2-Annulated Adamantane Heterocyclic Derivatives as Anti-Influenza A Virus Agents. Croat Chem Acta 2019; 92(2): 211-28.

[97] Fytas G, Zoidis G, Taylor MC, Kelly JM, Tsatsaroni A, Tsotinis A. Novel 2,6-diketopiperazine-derived acetohydroxamic acids as promising anti-*Trypanosoma brucei* agents. Future Med Chem 2019; 11(11): 1259-66.

[98] Kolocouris N, Zoidis G, Foscolos GB, *et al*. Design and synthesis of bioactive adamantane spiro heterocyles. Bioorg Med Chem Lett 2007; 17(15): 4358-62.

[99] Zoidis G, Tsotinis A, Kolocouris N, *et al*. Design and synthesis of bioactive 1,2-annulated adamantane derivatives. Org Biomol Chem 2008; 6(17): 3177-85.

[100] Zoidis G, Kolocouris N, Naesens L, De Clercq E. Design and synthesis of 1,2-annulated adamantane piperidines with anti-influenza virus activity. Bioorg Med Chem 2009; 17(4): 1534-41.

[101] Zoidis G, Kolocouris N, Kelly JM, Prathalingam SR, Naesens L, De Clercq E. Design and synthesis of bioactive adamantanaminoalcohols and adamantanamines. Eur J Med Chem 2010; 45(11): 5022-30.

[102] Fytas C, Zoidis G, Tzoutzas N, Taylor MC, Fytas G, Kelly JM. Novel lipophilic acetohydroxamic acid derivatives based on conformationally constrained spiro carbocyclic 2,6-diketopiperazine scaffolds with potent trypanocidal activity. J Med Chem 2011; 54(14): 5250-4.

[103] Zoidis G, Tsotinis A, Tsatsaroni A, *et al*. Lipophilic conformationally constrained spiro carbocyclic 2,6-diketopiperazine-1-acetohydroxamic acid analogues as trypanocidal and leishmanicidal agents: An extended SAR study. Chem Biol Drug Des 2018; 91(2): 408-21.

[104] Ulrich P, Cerami A. Trypanocidal 1,3-arylene diketone bis(guanylhydrazone)s. Structure-activity relationships among substituted and heterocyclic analogues. J Med Chem 1984; 27(1): 35-40.

[105] Bitonti AJ, Dumont JA, McCann PP. Characterization of *Trypanosoma brucei brucei S*-adenosyl-L-methionine decarboxylase and its inhibition by Berenil, pentamidine and methylglyoxal bis(guanylhydrazone). Biochem J 1986; 237(3): 685-9.

[106] Sundberg RJ, Dahlhausen DJ, Manikumar G, *et al*. Cationic antiprotozoal drugs. Trypanocidal activity of 2-(4'-formylphenyl)imidazo[1,2-a]pyridinium guanylhydrazones and related derivatives of quaternary heteroaromatic compounds. J Med Chem 1990; 33(1): 298-307.

[107] Messeder JC, Tinoco LW, Figueroa-Villar JD, Souza EM, Santa Rita R, de Castro SL, Aromatic guanyl hydrazones: Synthesis, structural studies and in vitro activity against *Trypanosoma cruzi*. Bioorg Med Chem Lett 1995; 5(24): 3079-84.

[108] Bacchi CJ, Brun R, Croft SL, Alicea K, Bühler Y. *In vivo* trypanocidal activities of new *S*-adenosylmethionine decarboxylase inhibitors. Antimicrob Agents Chemother 1996; 40(6): 1448-53.

[109] Brun R, Bühler Y, Sandmeier U, *et al*. *In vitro* trypanocidal activities of new *S*-adenosylmethionine decarboxylase inhibitors. Antimicrob Agents Chemother 1996; 40(6): 1442-7.

[110] Borges MN, Messeder JC, Figueroa-Villar JD. Synthesis, anti-*Trypanosoma cruzi* activity and micelle interaction studies of bisguanylhydrazones analogous to pentamidine. Eur J Med Chem 2004; 39(11): 925-9.

[111] Ellis S, Sexton DW, Steverding D. Trypanotoxic activity of thiosemicarbazone iron chelators. Exp Parasitol 2015; 150: 7-12.

[112] Papanastasiou I, Tsotinis A, Kolocouris N, Prathalingam SR, Kelly JM. Design, synthesis, and trypanocidal activity of new aminoadamantane derivatives. J Med Chem 2008; 51(5): 1496-500.

[113] Papanastasiou I, Tsotinis A, Zoidis G, Kolocouris N, Prathalingam SR, Kelly JM. Design and synthesis of *Trypanosoma brucei* active 1-alkyloxy and 1-benzyloxyadamantano 2-guanylhydrazones. ChemMedChem 2009; 4(7): 1059-62.

[114] Šekutor M, Mlinarić-Majerski K, Hrenar T, Tomić S, Primožič I. Adamantane-substituted guanylhydrazones: novel inhibitors of butyrylcholinesterase. Bioorg Chem 2012; 41-42: 28-34.

[115] Hirumi H, Hirumi K. Continuous cultivation of *Trypanosoma brucei* blood stream forms in a medium containing a low concentration of serum protein without feeder cell layers. J Parasitol 1989; 75(6): 985-9.

[116] Taylor MC, McLatchie AP, Kelly JM. Evidence that transport of iron from the lysosome to the cytosol in African trypanosomes is mediated by a mucolipin orthologue. Mol Microbiol 2013; 89(3): 420-32.

[117] Kendall G, Wilderspin AF, Ashall F, Miles MA, Kelly JM. *Trypanosoma cruzi* glycosomal glyceraldehyde-3-phosphate dehydrogenase does not conform to the 'hotspot' topogenic signal model. EMBO J 1990; 9(9): 2751-8.

[118] Sliwoski G, Kothiwale S, Meiler J, Lowe EW Jr, Computational methods in drug discovery. Pharmacol Rev 2014; 66(1): 334-95.

[119] Kapetanovic IM. Computer-aided drug discovery and development (CADDD): *in silico*-chemico-biological approach. Chem Biol Interact 2008; 171(2): 165-76.

[120] Baig MH, Ahmad K, Roy S, *et al*. Computer aided drug design: success and limitations. Curr Pharm Des 2016; 22(5): 572-81.

[121] Talele TT, Khedkar SA, Rigby AC. Successful applications of computer aided drug discovery: moving drugs from concept to the clinic. Curr Top Med Chem 2010; 10(1): 127-41.

[122] Lionta E, Spyrou G, Vassilatis DK, Cournia Z. Structure-based virtual screening for drug discovery: principles, applications and recent advances. Curr Top Med Chem 2014; 14(16): 1923-38.

[123] Macalino SJ, Gosu V, Hong S, Choi S. Role of computer-aided drug design in modern drug discovery. Arch Pharm Res 2015; 38(9): 1686-701.

[124] Erlanson DA. Introduction to fragment-based drug discovery. Top Curr Chem 2012; 317: 1-32.

[125] Tanaka D. [Fragment-based drug discovery: concept and aim]. Yakugaku Zasshi 2010; 130(3): 315-23.

[126] Bak A, Kozik V, Smolinskic A, Jampilekd J. Multidimensional (3D/4D-QSAR) probability-guided pharmacophore mapping: investigation of activity profile for a series of drug absorption promoters. RSC Adv 2016; 6(80): 76183-205.

[127] Devillers J. Methods for building QSARs. Methods Mol Biol 2013; 930: 3-27.

[128] Lavecchia A, Di Giovanni C. Virtual screening strategies in drug discovery: a critical review. Curr Med Chem 2013; 20(23): 2839-60.

[129] McGaughey GB, Sheridan RP, Bayly CI, *et al*. Comparison of topological, shape, and docking methods in virtual screening. J Chem Inf Model 2007; 47(4): 1504-19.

[130] Hart TN, Read RJ. A multiple-start Monte Carlo docking method. Proteins 1992; 13(3): 206-22.

[131] Irwin JJ, Shoichet BK. Docking screens for novel ligands conferring new biology. J Med Chem 2016; 59(9): 4103-20.

[132] Kitchen DB, Decornez H, Furr JR, Bajorath J. Docking and scoring in virtual screening for drug discovery: methods and applications. Nat Rev Drug Discov 2004; 3(11): 935-49.

[133] Li J, Fu A, Zhang L. An overview of scoring functions used for protein-ligand interactions in molecular docking. Interdiscip Sci 2019; 11(2): 320-328.

[134] Schrödinger Release 2018-1: Schrödinger Suite 2018-1 Protein Preparation Wizard; Epik, Schrödinger, LLC, New York, NY, 2018; Impact, Schrödinger, LLC, New York, NY, 2018; Prime, Schrödinger, LLC, New York, NY, 2018.

[135] Myrianthopoulos V, Lambrinidis G, Mikros E. *In silico* screening of compound libraries using a consensus of orthogonal methodologies. Methods Mol Biol 2018; 1824: 261-77.

[136] Schrödinger Release 2018-1: Ligprep, Schrödinger, LLC, New York, NY, 2018.

[137] Schrödinger Release 2018-1: Glide, Schrödinger, LLC, New York, NY, 2018.

[138] Friesner RA, Banks JL, Murphy RB, *et al*. Glide: a new approach for rapid, accurate docking and scoring. 1. Method and assessment of docking accuracy. J Med Chem 2004; 47(7): 1739-49.

[139] Friesner RA, Murphy RB, Repasky MP, *et al*. Extra precision glide: docking and scoring incorporating a model of hydrophobic enclosure for protein-ligand complexes. J Med Chem 2006; 49(21): 6177-96.

[140] Hansch C, Fujita T. p-σ-π Analysis. A method for the correlation of biological activity and chemical structure. J Am Chem Soc 1964; 86(8): 1616-26.

[141] Cherkasov A, Muratov EN, Fourches D, *et al*. QSAR modeling: where have you been? Where are you going to? J Med Chem 2014; 57(12): 4977-5010.

[142] Lill MA, Multi-dimensional QSAR in drug discovery. Drug Discov Today 2007; 12(23-24): 1013-7.

[143] Golbraikh A, Wang XS, Zhu H, Tropsha A. Predictive QSAR modeling: methods and applications in drug discovery and chemical risk assessment. In: Leszczynski J, Kaczmarek-Kedziera A, Puzyn T, Papadopoulos MG, Reis H, Shukla MK, Eds. Handbook of Computational Chemistry. Cham: Springer 2017; pp. 2303-40.

[144] Peter SC, Dhanjal JK, Malik V, Radhakrishnan N, Jayakanthan M, Sundar D. Quantitative structure-activity relationship (QSAR): modeling approaches to biological applications. Encycl Bioinforma Comput Biol 2019; 2: 661-76.

[145] Roy K, Kar S, Das RN. SAR and QSAR in drug discovery and chemical design—Some examples. Understanding the Basics of QSAR for Applications in Pharmaceutical Sciences and Risk Assessment, 2015; pp. 427-53.

[146] Schrödinger Release 2018-1: Canvas, Schrödinger, LLC, New York, NY, 2018.

[147] Sastry M, Lowrie JF, Dixon SL, Sherman W. Large-scale systematic analysis of 2D fingerprint methods and parameters to improve virtual screening enrichments. J Chem Inf Model 2010; 50(5): 771-84.

[148] Faulkner D, McKervey MA. The π-route to substituted adamantanes. Part I. J Chem Soc C 1971; 3906-10.

[149] Geluk HW, Schlatmann JLMA. Hydride transfer reactions of the adamantyl cation (IV): Synthesis of 1,4- and 2,6-substituted adamantanes by oxidation with sulfuric acid. Rec Trav Chim 1971; 88(13): 516-20.

[150] Hrdina R. Directed C–H functionalization of the adamantane framework. Synthesis 2019; 51(03): 629-42.

[151] Majerski Z, Hameršak Z. Rearrangement of bridgehead alcohols to polycyclic ketones by fragmentation-cyclization: 4-protoadamantanone (tricyclo-[4.3.1.0^{3,8}]decan-4-one). Org Synth 1988; 50: 958-62.

[152] Kolocouris N, Zoidis G, Fytas C. Facile synthetic routes to 2-oxo-1-adamantanalkanoic acids. Synlett 2007; 7(7): 1063-66.

[153] Chyi Tseng C, Handa I, Abdel-Sayed AN, Bauer L. N-[(aryl substitute adamantane)alkyl] 2-mercaptoacetamidines, their corresponding disulfides and 5-phosphorothioates. Tetrahedron 1988; 44(7): 1893-904.

[154] Endo Y, Sawabe T, Taoda Y. Electronic Effects of Icosahedral Carboranes. Retentive Solvolysis of (1,2-Dicarba-closo-dodecaboran-1-yl)benzyl p-Toluenesulfonates. J Am Chem Soc 2000; 122(1): 180-1.

[155] Natarajan A, Joy A, Kaanumalle LS, Scheffer JR, Ramamurthy V. Enhanced enantio- and diastereoselectivity via confinement and cation binding: yang photocyclization of 2-benzoyladamantane derivatives within zeolites. J Org Chem 2002; 67(24): 8339-50.

[156] Papanastasiou I, Tsotinis A, Kolocouris N, Nikas SP, Vamvakides A. New aminoadamantane derivatives with antiproliferative activity. Med Chem Res 2014; 23(4): 1966-75.

[157] Volkov OA, Kinch L, Ariagno C, et al. Relief of autoinhibition by conformational switch explains enzyme activation by a catalytically dead paralog. Elife 2016; 5: e20198.

[158] Schönherr H, Cernak T. Profound methyl effects in drug discovery and a call for new C-H methylation reactions. Angew Chem Int Ed Engl 2013; 52(47): 12256-67.

[159] Klebe G. Applying thermodynamic profiling in lead finding and optimization. Nat Rev Drug Discov 2015; 14(2): 95-110.

[160] Dunitz JD. Win some, lose some: enthalpy-entropy compensation in weak intermolecular interactions. Chem Biol 1995; 2(11): 709-12.

[161] Lumry R, Rajender S. Enthalpy-entropy compensation phenomena in water solutions of proteins and small molecules: a ubiquitous property of water. Biopolymers 1970; 9(10): 1125-227.

[162] Wienen-Schmidt B, Jonker HRA, Wulsdorf T, et al, Paradoxically, most flexible ligand binds most entropy-favored: intriguing impact of ligand flexibility and solvation on drug-kinase binding. J Med Chem 2018; 61(14): 5922-33.

[163] Motiejunas D, Wade RC. Structural, energetic, and dynamic aspects of ligand–receptor interactions, In: Triggle DJ, Taylor JB. Eds. Comprehensive Medicinal Chemistry II. Oxford: Elsevier 2007; pp. 193-213.

[164] Spyrakis F, Ahmed MH, Bayden AS, Cozzini P, Mozzarelli A, Kellogg GE. The roles of water in the protein matrix: a largely untapped resource for drug discovery. J Med Chem 2017; 60(16): 6781-827.

[165] SZMAP, 1.2.1 OpenEye Scientific Software Inc. , Santa Fe, NM, USA, 2015.

[166] Bayden AS, Moustakas DT, Joseph-McCarthy D, Lamb ML. Evaluating free energies of binding and conservation of crystallographic waters using SZMAP. J Chem Inf Model 2015; 55(8): 1552-65.

[167] Myrianthopoulos V, Gaboriaud-Kolar N, Tallant C, et al. Discovery and optimization of a selective ligand for the switch/sucrose nonfermenting-related bromodomains of polybromo protein-1 by the use of virtual screening and hydration analysis. J Med Chem 2016; 59(19): 8787-803.

[168] Todeschini R, Consonni V. Handbook of Molecular Descriptors. Methods and Principles in Medicinal Chemistry. 2000: WILEY-VCH Verlag GmbH.